# The Olivine-Melt Equilibrium Method for Determining Oxygen Fugacity

Senior Thesis

Presented in Partial Fulfillment of the Requirements for
the Bachelor of Sciences Degree *with Research Distinction* in Geological Sciences
in the undergraduate colleges of The Ohio State University

By

Kenneth J. Peterman
The Ohio State University
2015

Approved By

Dr. Michael Barton, Project Advisor

School of Earth Sciences

# TABLE OF CONTENTS

# Acknowledgments

I would like to thank my research advisor, Dr. Michael Barton, for suggesting this research project, for reviewing the results, and for providing insightful feedback on many components of this thesis. I truly appreciate this research opportunity because it has improved my ability think as a scientist and it is an excellent way to express my enthusiasm for the Earth Sciences. I am grateful that this research will give me the memorable opportunity to travel to Iceland in order to collect my own samples. This will absolutely benefit this research as I continue to transition into my master's program. I would like to thank my parents and my fiancée for doing anything they possibly can in order to support my enthusiasm for the Earth Sciences.

I would also like to thank the following scholarships for lessening the financial burden of college: the Sheila Brannon Scholarship, the Licking County Foundation Scholarship, the Name and Seal Scholarship, the Scarlet and Grey Grant, the SES Field Experience Travel Fund, the Stark County Gem and Mineral Club Scholarship, and the Rector Scholarship Fund.

# Abstract

In order to connect volcanic rocks and their mantle sources, it is essential to consider redox equilibria and their dependence on temperature, pressure, composition, and oxygen fugacity. Oxygen fugacity plays a very important role in determining which minerals can crystallize and coexist in a rock, and therefore it is possible to determine the oxygen fugacity at which a particular rock equilibrates from chemical analyses of coexisting minerals and melt. The olivine-melt equilibrium method has been developed at The Ohio State University in order to calculate oxygen fugacity. First, the ferric to ferrous iron ratio of the melt must be determined. This ratio expresses the valence state of iron and hence the redox state of the magma. This ratio can be determined from the compositions of co-existing olivine and melt equilibrium pairs using the distribution coefficient describing the partitioning of magnesium and ferrous iron between olivine and liquid. The calculated ferric to ferrous iron ratios of the melt can then be used to calculate the oxygen fugacity at which the magma equilibrated. Hundreds of samples containing volcanic glass and coexisting olivine phenocrysts have been processed with the olivine-liquid equilibrium method for determining oxygen fugacity. The compositional data from these samples were retrieved from published research articles. The results for Iceland yielded average oxygen fugacities between 0 and -1 log unit below the Fayalite-Magnetite-Quartz (FMQ) buffer. The Mid-Atlantic Ridge gives an average of -1.6 log units below the FMQ buffer. The olivine-melt equilibrium method can be applied to many volcanic rocks from other tectonic environments in order to compare the redox state of magmas, global variations in magma and hence mantle redox states, and to determine how mantle redox states have varied through time.

# 1. Introduction

Oxygen fugacity plays a very important role in determining which minerals can crystallize from magmas and which minerals can coexist in igneous rocks. In principle, it is possible to determine the oxygen fugacity at which a particular magma crystallizes from analyses of the minerals in equilibrium with the melt. Moreover, the oxygen fugacities of basaltic magmas reflect those of the mantle source regions, and it is therefore essential to consider redox equilibria and their dependence on temperature, pressure, composition, and oxygen fugacity to understand both the origin and evolution of magmas.

A number of methods have been used to determine the oxygen fugacities of lavas, including methods based on mineral equilibria involving two-oxides (Buddington and Lindsley, 1964; Anderson and Lindsley, 1988; Anderson et al., 1991; Ghiorso and Sack, 1991) or oxide-silicate assemblages (Ballhaus et al., 1990, 1991; Frost et al., 1988; Lindsley et al., 1990; Ghiorso and Sack, 1991; Lindsley and Frost, 1992; Frost and Lindsley, 1992). These methods do not work well for basalt – the most abundant magma on earth, which lacks appropriate mineral assemblages. Another method is based on analyzed $Fe^{3+}/\sum Fe$ of glassy samples (Christie et al., 1986; Carmichael and Ghiorso, 1986; Carmichael, 1991; Kress and Carmichael, 1991). However, determination of $Fe^{3+}$ and $Fe^{2+}$ by wet chemical techniques is time consuming and requires careful analytical procedures (Bézos and Humler, 2005). The number of laboratories using these techniques is declining (Carmichael and Ghiorso, 1990) and other methods to determine $Fe^{3+}$ and $Fe^{2+}$ (such as mössbauer spectroscopy and K-edge micro-XANES spectroscopy (Delaney et al., 1996)) are not yet widely used by petrologists or geochemists to analyze glasses due to the difficult process of analyzing samples. It is therefore unlikely that use

of $Fe^{3+}/\Sigma Fe$ to estimate $fO_2$ will be widespread amongst petrologists and geochemists in the near future.

A novel method to determine $fO_2$ has been developed and is based on olivine-melt equilibrium (Barton, 2003; Miller et al., 2005). This method has the advantage that olivine and glass (or groundmass) compositions are determined by electron probe micro analyzer (EPMA) so that specialized analytical equipment is not required, and olivine compositions are routinely determined in petrologic studies to constrain petrogenetic models. The purpose of the research described in this thesis is to use the olivine-melt method to determine the oxygen fugacities at which basalt magmas erupted along the Mid-Atlantic Ridge crystallized. The objective is to test whether the olivine-melt method yields results that are consistent with those obtained in previous studies using different methods, and to ascertain whether there is significant variation in the redox states of the mantle source regions of Mid-Ocean Ridge basalts.

### *1.1 Oxygen Fugacity*

In the early 20th century, a physical chemist named G.N. Lewis invented a function he called fugacity, which was derived from the Latin root meaning "to escape" (Lewis, 1901). Fugacity is a measure of the escaping tendency of a real gas from a solution. In many petrologic applications when pressures exceed one bar, real gases deviate significantly from ideal behavior. Therefore, fugacity is necessary to express the thermodynamic partial pressure of a real gas in these particular conditions (Faure, 1998).

Oxygen fugacity is a convenient parameter used to monitor the oxidation state of a system. This property measures the availability of oxygen to participate in chemical reactions, and gives information regarding whether iron, for example, is likely to be found in its native

state, as a divalent ion in a silicate mineral, or as a divalent or trivalent ion in an oxide mineral (Lindsley, 1991). Small changes in oxygen fugacity can drastically affect the pathway of magmatic differentiation and of fractional crystallization. These changes in mineral assemblages resulting from changes of oxygen fugacity are mostly the result of the change in the oxidation state of iron (Philpotts, 2009).

In 1935, Bowen and Schairer studied the relationship between oxide minerals and ferromagnesian silicates. They observed that ferrous iron crystallizes in relatively reduced conditions, whereas ferric iron crystallizes in more oxidized conditions (Bowen and Schaierer, 1935). High oxygen fugacities are responsible for early crystallization of magnetite. This phenomenon yields residual liquids depleted in FeO and rich in $SiO_2$, therefore it is referred to as the silica-enrichment trend, or calc-alkaline trend (Frost and Lindsley, 1992). The iron-enrichment trend, or tholeiitic trend, occurs at low oxygen fugacities, which suppresses early crystallization of magnetite and yields residual liquids rich in FeO at nearly constant $SiO_2$ (Frost and Lindsley, 1992). These different trends can be appreciated by considering Le Châtelier's Principle and the following chemical reaction:

$$\underset{\text{Fayalite}}{3Fe_2SiO_4} + \underset{\text{Gas}}{O_2} \rightleftharpoons \underset{\text{Magnetite}}{2Fe_3O_4} + \underset{\text{Quartz}}{3SiO_2} \quad \text{..... (Eq. 1)}$$

Where increases in $fO_2$ push the equilibrium reaction to the right, in order to reestablish equilibrium conditions, thereby resulting in a silica-enrichment trend. Low $fO_2$ pushes the reaction to the left, which favors crystallization of fayalitic olivine due to the iron-enrichment trend.

### *1.2 Buffers*

Hans Eugster first introduced the concept of oxygen controlling equilibria, or oxygen buffers, in 1957 (Eugster, 1957). The term "buffer" is appropriate because the oxygen fugacities of these univariant mineral assemblages have a single value at a fixed temperature and total pressure. This is due to the fact that the equilibrium constants for these redox reactions are written only as a function of oxygen fugacity. Therefore, while the reduced and oxidized mineral assemblages are in equilibrium, the oxygen fugacity is fixed at a particular temperature and total pressure (Nordstrom and Munoz, 1994). However, as the temperature increases, the oxygen fugacity of all buffers also increases (Figure 1). This reflects the fact that devolatilization reactions occur more readily at higher temperatures, which results in more oxygen escaping, which increases oxygen fugacity (Lindsley, 1991). These particular buffers are mineral assemblages involved in redox reactions that were used to control oxygen fugacity in experiments. However these mineral assemblages rarely exist together in nature. For example, most igneous rocks crystallize near the fayalite-magnetite-quartz buffer:

$$\underset{\text{Fayalite}}{3Fe_2SiO_4} + \underset{\text{Gas}}{O_2} \rightleftharpoons \underset{\text{Magnetite}}{2Fe_3O_4} + \underset{\text{Quartz}}{3SiO_2} \quad \text{..... (Eq. 2)}$$

However, very few igneous rocks contain these coexisting minerals in abundance (Philpotts, 2009). Rare locations with very iron-rich igneous rocks may contain this mineral assemblage, such as the Skaergaard and Bushveld igneous complexes (Barton, personal communication, 2015).

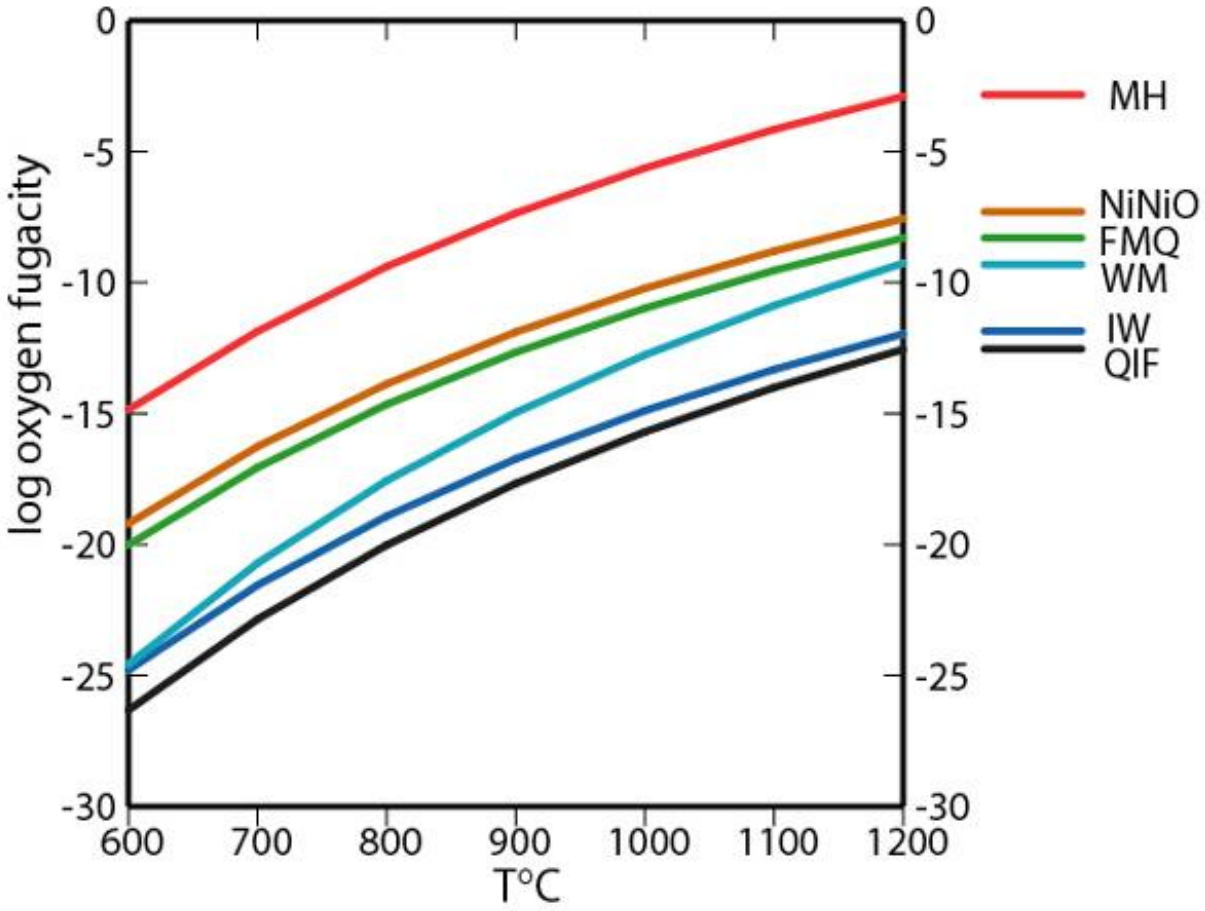


**Figure 1**: log($fO_2$) is plotted against temperature for various buffers at one bar based on specific algorithms. These buffers include: MH: magnetite-hematite ($4Fe_3O_4 + O_2 \leftrightarrow 6Fe_2O_3$); NiNiO: nickel-nickel oxide ($2Ni + O_2 \leftrightarrow 2NiO$); FMQ: fayalite-magnetite-quartz ($3Fe_2SiO_4 + O_2 \leftrightarrow 2Fe_3O_4 + 3SiO_2$); WM: wüstite-magnetite ($3Fe_{1-x}O + O_2 \leftrightarrow Fe_3O_4$); IW: iron-wüstite ($2(1-x)Fe + O_2 \leftrightarrow 2Fe_{1-x}O$); QIF: quartz-iron-fayalite ($2Fe + SiO_2 + O_2 \leftrightarrow Fe_2SiO_4$). (Lindsley, 1991)

Most igneous rocks crystallize near the fayalite-magnetite-quartz (FMQ) buffer; therefore oxygen fugacity is commonly reported as a deviation from this buffer in log units. Most mafic igneous rocks equilibrate at oxygen fugacities about one log unit below the FMQ buffer (Lindsley, 1991). Few mafic rocks equilibrate two log units below FMQ, and very rare mafic rocks with native iron crystallize up to greater than four units below the FMQ buffer (Lindsley, 1991). Most felsic rocks crystallize approximately one to two log units above FMQ, and few silicic igneous rocks crystalize greater than three log units above FMQ (Lindsley, 1991). Metamorphic rocks have a wider range of oxygen fugacities compared to igneous rocks due to the fact that there is a much wider range of bulk compositions of metamorphic rocks (Lindsley, 1991).

### *1.3 The Quartz-Ulvöspinel-Ilmenite-Fayalite Method*

The equilibria involved in these buffer reactions (Figure 1) illustrate the fact that oxygen fugacity places restrictions on what minerals can coexist and crystalize from certain melts. In other words, oxygen fugacity plays an important role in determining which minerals can crystallize and coexist in a rock. For example, there are no conditions on Earth in which hematite and fayalite can coexist and crystallize together (Philpotts, 2009). On the other hand, it is possible to determine the oxygen fugacity at which a particular rock equilibrated from its mineral assemblage (Philpotts, 2009).

A common method for determining oxygen fugacity is the quartz-ulvöspinel-ilmenite-fayalite (QUILF) method explained by Frost et al. (1988), Frost and Lindsley (1992), and Lindsley and Frost (1992). This method involves the equilibrium:

$$SiO_2 + 2Fe_2TiO_4 \rightleftharpoons 2FeTiO_3 + Fe_2SiO_4$$
Quartz Ulvöspinel Ilmenite Fayalite ..... (Eq. 3)

Igneous rocks may contain both the ilmenite-hematite solid solution, referred to as the rhombohedral phase; as well as the magnetite-ulvöspinel solid solution, known as the spinel phase (Philpotts, 2009). Therefore, it is possible to determine the oxygen fugacity and temperature at which these igneous rocks equilibrated, as long as the rock contains both of these phases (Philpotts, 2009). At low oxygen fugacities, the spinel phase is ulvöspinel-rich, and coexists with an ilmenite-rich rhombohedral phase (Philpotts, 2009). As the oxygen fugacity increases, the spinel phase becomes more magnetite-rich (Philpotts, 2009). At relatively high oxygen fugacities, the spinel phase is magnetite-rich, and the rhombohedral phase contains hematite (Philpotts, 2009). The QUILF method constrains estimates of oxygen fugacity and demonstrates that oxide and silicate compositions are interrelated. However, this mineral assemblage must be present in order to calculate the oxygen fugacity and this assemblage is not always present in basalts (Frost and Lindsley, 1992; Lindsley and Frost, 1992). Therefore it is desirable to develop another method to determine the oxygen fugacities of magmas.

# 2. Methodology

Another method used to calculate oxygen fugacity has been developed at The Ohio State University School of Earth Sciences by Barton (2003) in which olivine-melt equilibrium can be utilized to determine oxygen fugacity. This method involves the relationship between coexisting olivines and the melt. Olivine is among the first phases to crystallize among basalts of different chemical compositions. It has a complete solid solution between iron and magnesium end-members: fayalite ($Fe_2SiO_4$) and forsterite ($Mg_2SiO_4$), where the olivine is typically richer in magnesium and poorer in iron compared to the coexisting melt (Roeder and Emslie, 1970). First, the ferric to ferrous iron ratio of the melt must be determined. This ratio expresses the dominant valence states of iron, and hence the redox state of the magma. The ratio can be determined from the compositions of co-existing olivine and melt equilibrium pairs using the distribution coefficient describing the partitioning of magnesium and ferrous iron between olivine and liquid. The calculated ferric and ferrous iron contents of the melt can then be used to calculate the oxygen fugacity at which magma equilibrated.

### *2.1 Exchange of MgO and FeO between Olivine and Liquid*

In 1970, two Canadian geologists named Roeder and Emslie researched magnesium and ferrous iron distribution between olivine and melt, given by the equation:

$$\mathrm{Mg_{Ol}} + \mathrm{Fe^{2+}_{Liq}} \rightleftharpoons \mathrm{Mg_{Liq}} + \mathrm{Fe^{2+}_{Ol}} \quad \text{..... (Eq. 4)}$$

They experimentally determined a distribution coefficient ($K_D$) that relates the partitioning of iron and magnesium between the olivine and the liquid:

$$K_D = \frac{X_{FeO}^{Ol}}{X_{FeO}^{Liq}} \frac{X_{MgO}^{Liq}}{X_{MgO}^{Ol}} = 0.3 \pm 0.03 \quad \text{..... (Eq. 5)}$$

Where X are the mole fractions of iron and magnesium in the olivine and the liquid (Roeder and Emslie, 1970). The distribution coefficient was determined to be equal to 0.30 ± 0.03, and remained nearly constant at various temperatures, compositions, and oxygen fugacities during this study (Roeder and Emslie, 1970). If the distribution coefficient determined for a particular olivine-melt pair does not fall in this range (0.3±0.03), then it is almost certain that the olivine did not crystallize from the host liquid. Therefore, it is most likely an olivine xenocryst (Roeder and Emslie, 1970). Figure 2 shows olivine compositions calculated from the melt composition using $K_D = 0.30$ compared to actual olivine data for the same samples. There is clearly satisfactory agreement between calculated and observed olivine compositions, supporting the use of the Roeder-Emslie equation to describe the partitioning of ferrous iron and magnesium between olivine and melt.

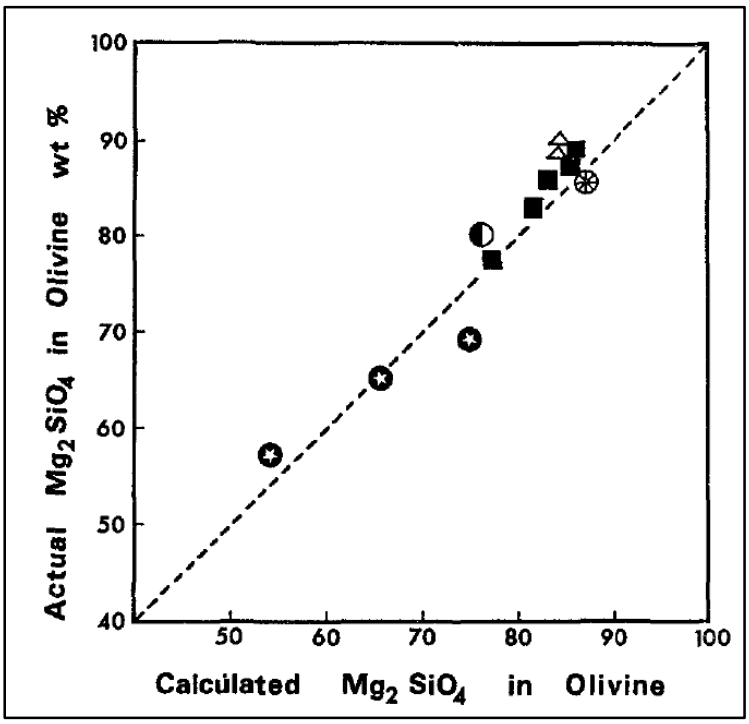


**Figure 2**: The actual forsterite weight percentage in olivine vs. the calculated forsterite weight percentage in olivine, using $K_D = 0.30$. Several experimental data are plotted. Both the actual data and calculated data agree very well with each other. (Roeder and Emslie, 1970)

The variation in the value of the distribution coefficient as a function of temperature is given by Roeder and Emslie (1970) as:

$$\log(K_D) = \frac{130}{T} - 0.7044 \quad \text{..... (Eq. 6)}$$

Variation in $K_D$ is relatively small at high temperatures (1150 to 1300°C for their study). This is the consequence of the small value for the numerator (130), which reflects the similar enthalpies of fusion of forsterite and fayalite (Roeder and Emslie, 1970). Therefore, the distribution coefficient is essentially constant regardless of temperature variations over the range expected for basaltic magmas, as seen in Figure 3. The experiments performed by Roeder and Emslie (1970) also demonstrated that although the composition of olivine is dependent on oxygen fugacity, the value of the distribution coefficient is independent of oxygen fugacity (Figure 4).

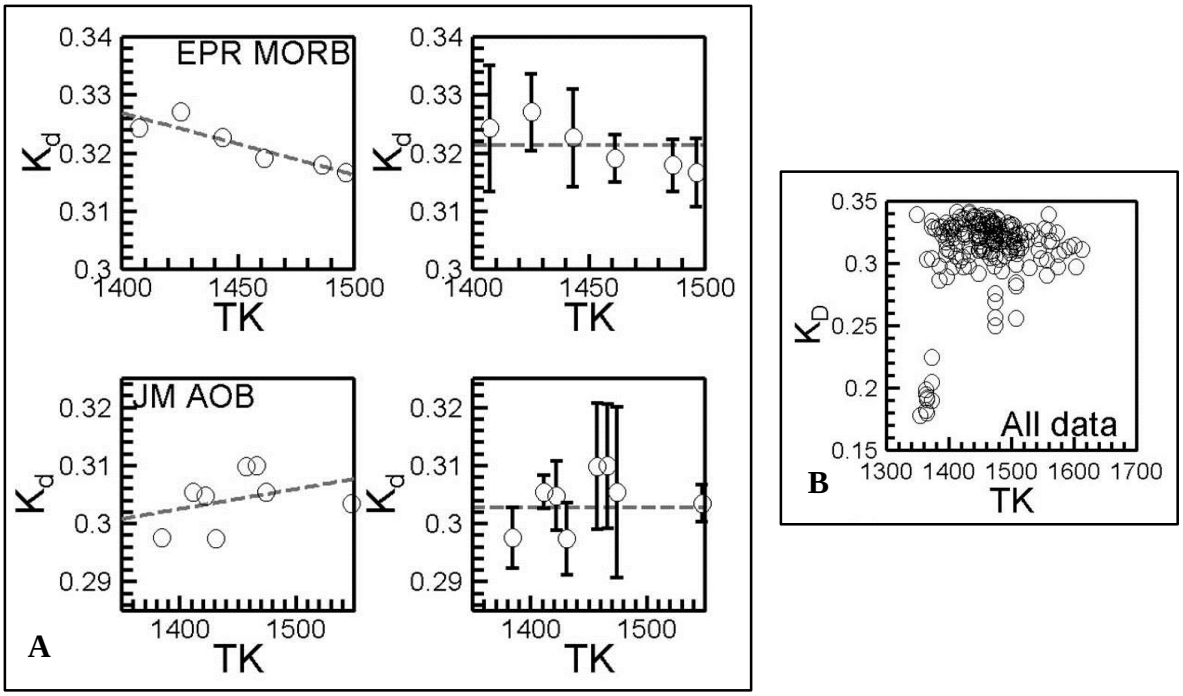


**Figure 3a:** $K_D$ is plotted against temperature (in Kelvin) at which the samples equilibrated for various samples. The error bars are plotted on the right two graphs, which displays there is no correlation between the $K_D$ and temperature of these samples (Barton, unpublished data, 2014).

**Figure 3b:** $K_D$ is plotted against temperature for many different samples (Barton, unpublished data, 2014). There is no correlation between $K_D$ and temperature, and $K_D$ is independent of temperature as demonstrated by Roeder and Emslie (1970).

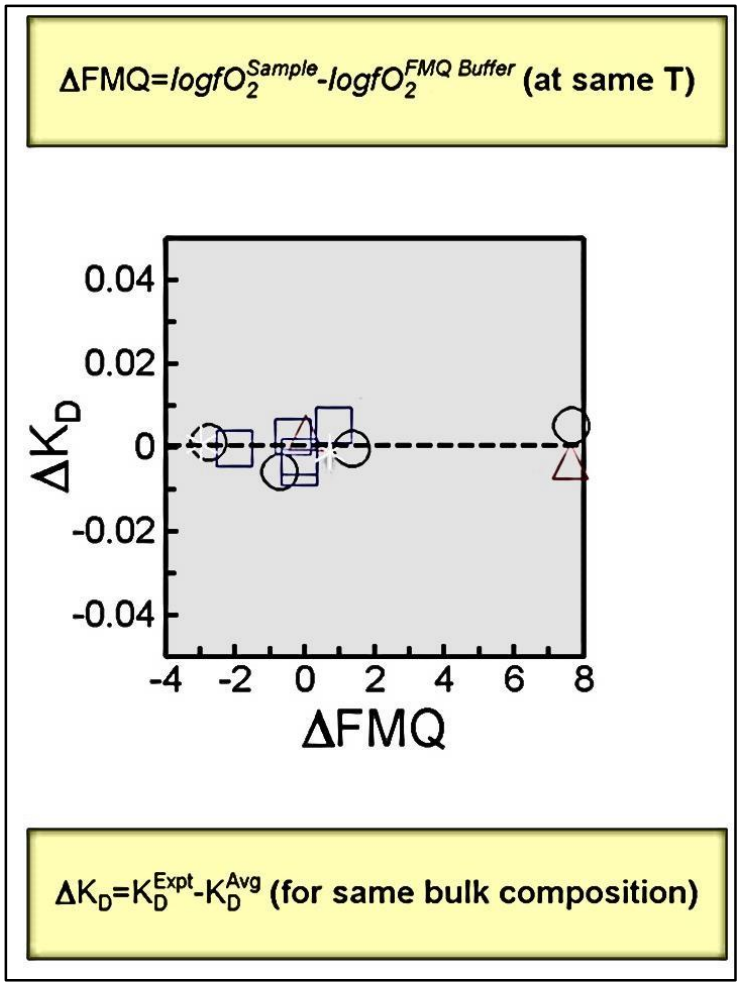


**Figure 4:** Deviation in $K_D$ plotted against the deviation in log($fO_2$) relative to the FMQ buffer for various samples and oxygen fugacities. This shows that the distribution coefficient and oxygen fugacity are independent of one another (Barton, unpublished data, 2014).

There is a relatively large uncertainty in the value of the distribution coefficient, (±0.03) (Roeder and Emslie, 1970). This may be the result of using older analysis of olivine and glass with electron microprobes that are less accurate and precise compared to modern instrumentation (Barton, unpublished writing, 2014). Another source of the uncertainty in the distribution coefficient may stem from uncertainties on the influence of melt composition. In other words, this relatively large variation in $K_D$ may reflect the wide variation in chemical compositions used in order to determine it. This uncertainty of 0.03 is responsible for an uncertainty up to 3 mol%

forsterite; therefore the true equilibrium olivine-melt composition is not very well constrained (Barton, unpublished writing, 2014).

Longhi et al. (1978) confirmed the work of Roeder and Emslie, showing that the distribution coefficient was equal to 0.30 plus or minus 0.03, but showed that it is independent of temperature. They did this by analyzing the distribution of iron and magnesium between coexisting olivine and different lunar basaltic liquids. However, they suggested that the distribution coefficient varies with changes in liquid chemistry (Longhi et al., 1978). The distribution coefficient varies with changes in silica concentration, even though it is strictly independent of silica activity by definition (Longhi et al., 1978). Longhi et al. (1978) suggested that the change in $K_D$ with composition is the result of the influence of silica concentration on the mixing properties of iron and magnesium in liquids with different chemistry. They suggested that the magnesium activity increases with increasing degrees of polymerization of the melts. These variations in $K_D$ can be accounted for by empirical corrections to the expression for $K_D$ to take into account variations in silica activity (Longhi et al., 1978).

In 1988, Gee and Sack observed that the value of the distribution coefficient varies with the amount of silica and alkalis in the melt. Their experiment involved experimental studies of multiple saturated liquids at low pressures (1 atmosphere) (Gee and Sack, 1988). These liquids crystallized coexisting nepheline, leucite, and spinel with or without olivine, Ca-rich pyroxene, and melilite (Gee and Sack, 1988). These workers concluded that the distribution coefficients for olivine and Ca-rich clinopyroxene are sensitive to melt chemistry unlike the distribution coefficient for melilite, which is relatively constant (Gee and Sack, 1988). Gee and Sack (1988) found that the value of the distribution coefficient for Mg and $Fe^{2+}$ between olivine and melt decreases as alkalinity increases. In other words, the value of $K_D$ decreases as the compositions

of the melts change from tholeiite to alkali basalt, to ugandite, to melilite nephelinite. They defined this compositional dependence of $K_D$ using pseudoternary liquidus projections in the system the CaO-MgO-$Al_2O_3$-$SiO_2$ (CMAS), where:

$$\ln(K_D) = -6.06 + 8.104\left[\frac{S}{(S + CA + M)}\right] - 4.742\left[\frac{S}{(S + CA + M)}\right]^2 \quad \text{..... (Eq. 7)}$$

Toplis (2005) agreed with Gee and Sack (1988) that it was an oversimplification to state that $K_D$ = 0.30 for a range of liquid (and olivine) compositions, because melt chemistry does in fact influence the value of $K_D$.

McCann (personal communication, 2015) has tested the various models for $K_D$ using olivine-melt pair produced in experiments on natural basalts. Her research demonstrates that the expression reported by Gee and Sack (1988) best describes the compositional dependence of $K_D$ and allows olivine compositions in equilibrium with melt, and vice-versa, to be calculated accurately (i.e. the error associated with $K_D$ is ~±0.008 compared to the value of ±0.03 determined by Roeder and Emslie (1970)).

### *2.2 Relationship between FeO, $Fe_2O_3$, and $fO_2$*

Kilinc et al. (1983) and Kress and Carmichael (1991) defined the relationship between $(Fe_2O_3/FeO)^{Melt}$, oxygen fugacity, temperature, and melt composition. They found that oxygen fugacity can be determined from ferric to ferrous iron ratios by the equation:

$$\ln\left(\frac{X_{Fe_2O_3}}{X_{FeO}}\right)^{Melt} = a\ln(fO_2) + \frac{b}{T} + c + \Sigma\, d_i X_i \quad \text{..... (Eq. 8)}$$

Where a, b, c, and $d_i$ are constants determined by step-wise linear regression analysis using experimental data, and $X_i$ is the mole fraction of component i in the melt. Values for the constants are given by Kilinc et al. (1983) and Kress and Carmichael (1991).

### *2.3 Calculation of Oxygen Fugacity from Olivine-Melt Equilibrium*

The olivine-melt equilibrium method for determining oxygen fugacity originally described by Barton (2003) has been refined in subsequent work (Barton, personal communication, 2014). This method is used to determine the ferric to ferrous iron ratios of the melt, which is essential for calculating oxygen fugacity. The method is illustrated in Figure 5 and is based on the fact that variations in the melt redox state and oxygen fugacity affect the stability and composition of the coexisting olivine solid solutions (Barton, unpublished writing, 2014). These are important parameters when modeling the characteristics of residual liquids created during magma crystallization. Kress and Carmichael (1991) have also determined experimentally that there will be little driving force for chemical diffusion of oxygen into or out of the melt phase. Therefore, only crystallization of iron-rich phases, vapor fractionation, or magma interaction with its surroundings of drastically different redox states will change the ΔFMQ of the melt during magma evolution (Kress and Carmichael, 1991). However, as magma adiabatically ascends and decompresses in a closed system, the oxidation state of the melt will not change and will reflect the magma source region (Kress and Carmichael, 1991).

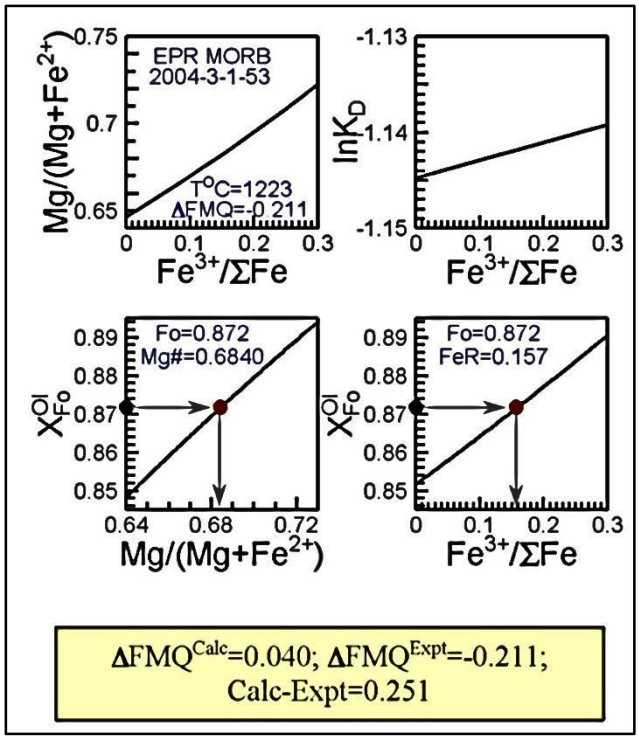


**Figure 5:** Using olivine-melt equilibrium (with ΣFe=FeO for the melt) to fix $(Fe^{3+}/\Sigma Fe)^{Melt}$ (Barton, unpublished data, 2014). The $(Fe^{3+}/\Sigma Fe)^{Melt}$ is then used to calculate $fO_2$.

Many compositional data are obtained via electron microprobe, but this instrument cannot distinguish between ferric and ferrous iron. As a result, probe analyses report total iron only as FeO. However, the actual value of FeO in the melt can be calculated from the composition of the olivine and knowledge of $K_D$. If the distribution coefficient is fixed, and the molar fractions of forsterite, fayalite, and MgO in the melt are analyzed, this only leaves one unknown variable that can be solved for: the FeO in the liquid. The difference between the total (analyzed) FeO and calculated FeO gives the amount of $Fe_2O_3$.

$$FeO + Fe_2O_3 = \Sigma Fe \quad \text{..... (Eq. 9)}$$

$$\Sigma Fe \text{ (analyzed)} - FeO \text{ (calculated)} = Fe_2O_3 \quad \text{..... (Eq. 10)}$$

Hence, the ferric to ferrous iron ratio of the melt is in fact known, and can be used to calculate oxygen fugacity using equation 8 described by Kress and Carmichael (1991).

The olivine-liquid equilibrium program written by Barton is a Microsoft Excel program that requires weight percentages of the major oxides of volcanic glasses, typically analyzed via electron microprobe. Fresh, unaltered, crystal-poor, glassy lavas are the best indicators of the relative oxidation state of magma source regions because they represent a snapshot of equilibrium conditions of the liquid (Kress and Carmichael, 1991). Analyses of coexisting olivines are then necessary in order to determine the mole percent of forsterite of the olivine phenocrysts in equilibrium with the melt. The temperature at which the melt equilibrated is also required, which is calculated (assuming anhydrous conditions) from the glass analyses using the geothermometer program developed by Sugawara (2000). These compositional data are run through the excel program written by Dr. Barton, which employs the distribution coefficient developed by Gee and Sack (1988) that accounts for compositional variations. The $K_D$ is then used to calculate the ferric to ferrous iron ratio, which is used to calculate oxygen fugacity in the equation given by Kress and Carmichael (1991).

### *2.4 Application to Natural Samples*

In this study, hundreds of samples containing volcanic glass and coexisting olivine phenocrysts have been processed with the olivine-liquid equilibrium method for determining oxygen fugacity. The compositional data from these samples were retrieved from published research articles (Breddam, 2002; Thomson and Maclennan, 2013; Laubier et al., 2012) and datasets from PetDB and Geomapapp. The samples are from two locations along the Mid-Atlantic Ridge: Iceland and the FAMOUS Region. The geology of these locations is described in the following section.

# 3. Geologic Setting

### *3.1 Iceland*

Iceland is a significant setting for the application of the olivine-melt equilibrium method to determine oxygen fugacity because of its unique setting. Iceland is located at the intersection of the Mid-Atlantic Ridge and the Greenland-Iceland-Faeroe Ridge, and is the only place on Earth where the Mid-Ocean Ridge is above sea level. Seismic and geochemical data suggest the presence of a mantle plume located beneath Iceland, although the existence of a plume is debated by some (Thordarson and Larsen, 2007). Nevertheless, the presence of a mantle plume is perhaps the best explanation of Iceland's anomalous elevation at 3,000 m above the surrounding sea floor (Thordarson and Larsen, 2007). Iceland's crustal thickness varies between 10 km and 40 km (Leftwich et al., 2005). This is extremely anomalous compared to most oceanic crust, which is approximately 7 ± 1 km thick on average (Bown and White, 1994). Only 30% of the landmass is exposed above sea level; however the addition of the submarine landmass covers about 350,000 $km^2$ (Thordarson and Larsen, 2007).

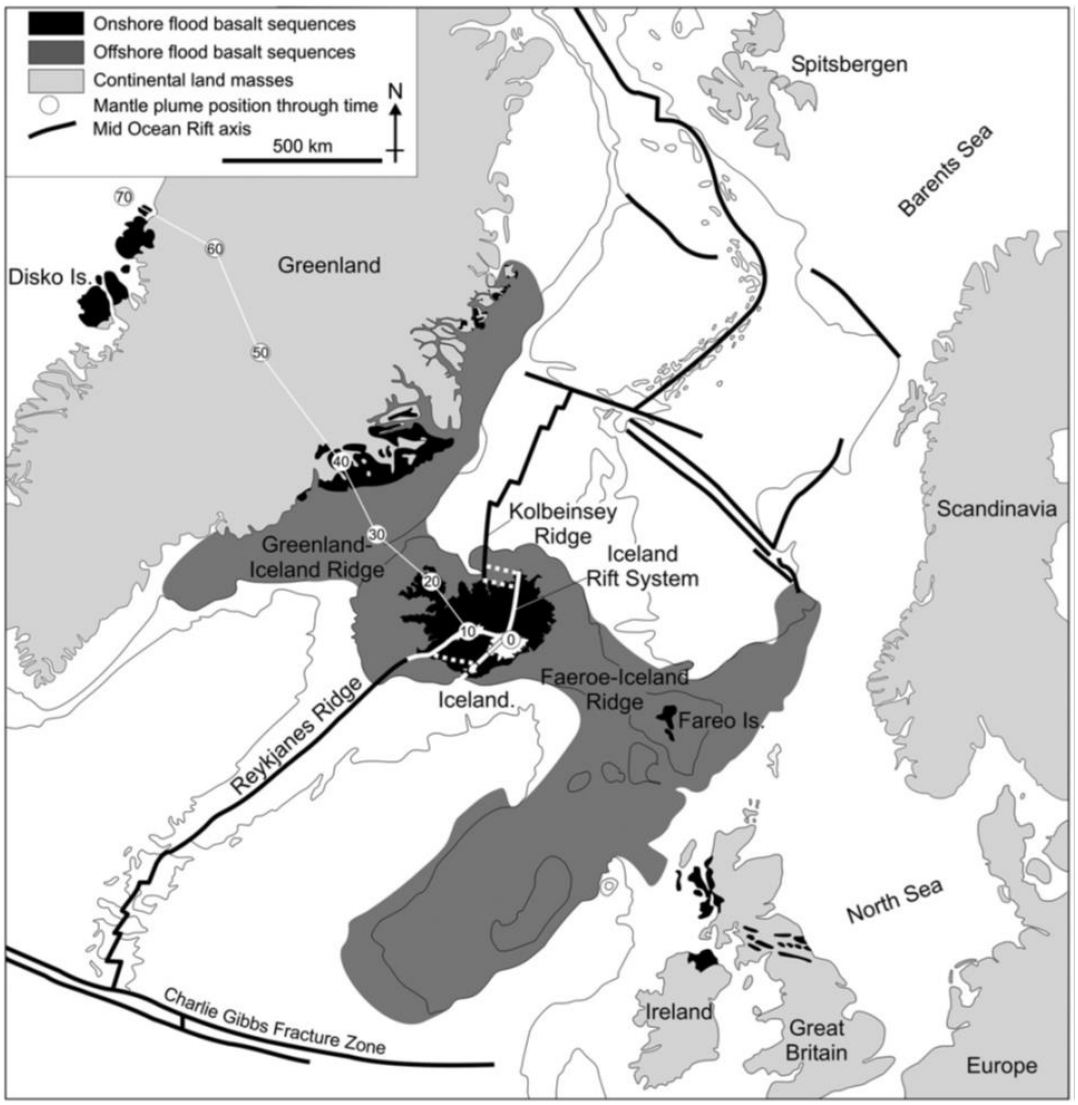


**Figure 6:** Iceland's position between the Reykjanes and Kolbeinsey Ridge. The Mid-Atlantic Ridge axis is displayed as a solid black line. The white dots, indicating age in Ma, show the position of the mantle plume relative to the lithosphere, and how it has varied position in the past 65 Ma. The North Atlantic basalt plateau and their submarine equivalents are also shown in black and grey respectively (Thordarson and Larsen, 2007).

The oldest rocks on Iceland are only 14 to 16 million years old, however its construction is believed to have initiated about 24 million years ago through multiple eruptive phases (Thordarson and Larsen, 2007). The Iceland mantle plume is hypothesized to have been active for the last 65 million years, and is responsible for constructing the nearly 2,000 km long North Atlantic Igneous Province, in which Iceland is located. Iceland is the only part of this province that is currently active (Thordarson and Larsen, 2007).

About 205 volcanic eruptions have occurred during recorded history. The timing of the eruptions have been identified by using dating methods, and by various documents that record eruptive events (Thordarson and Larsen, 2007). Of these 205 volcanic eruptions, the majority, 192, are simply individual eruptive events. The remaining 13 eruptions are defined as fires, which occur as several eruptions that may last for many months, or even years. Of these 13 fires, 8 were effusive eruptions, while the other 5 were explosive, creating many layers of tephra (Thordarson and Larsen, 2007). The 8 month long flood basalt eruption of Laki is considered a fire, for example. The Laki eruption occurred between June 8, 1783 and February 7, 1784, along part of the Grímsvötn volcanic system located in Iceland's Eastern Volcanic Zone (Passmore et al., 2012). The Laki event was the second largest volcanic eruption in Iceland's recorded history, after the AD 934 to AD 938 Eldgjá flood basalt event. Many earthquakes preceded the eruption for several weeks and were recorded by the local inhabitants. Over its 8 months of activity, Laki produced about 14.7 $km^3$ of quartz-tholeiite basalt plus 0.4 $km^3$ of tephra from 10 en echelon fissures (Thordarson and Larsen, 2007). The flood basalts cover an area of over 600 $km^2$, stretching from Vatnajökull's southwest boundary to Iceland's southern coast (Passmore et al., 2012). Such flood basalts can potentially drastically affect the environment, as well as society. Dating of the eruptive events that have occurred during human history gives volcanic eruption

recurrence frequencies of 20 to 25 per century; however this interval is likely variable because it is only a snapshot of geologic time, as well as a very small fraction of the age of Iceland (Thordarson and Larsen, 2007).

The primary regions of active volcanism occur where the Mid-Atlantic Ridge is superimposed on top of the mantle plume. The arrangement of these volcanic regions depends on the location and direction of movement of the tectonic plates over the mantle plume, as well as the movement of the spreading plate boundary. The location of plate construction and spreading is known as the axial volcanic zone. This constructive boundary can be traced all of the way across Iceland, from the Reykjanes Peninsula in the southwest to Öxarfjörður in the northern part of the island. There are 4 primary large scale volcanic zones, and 30 smaller scale volcanic systems in Iceland: The West Volcanic Zone (WVZ) with 6 volcanic systems, North Volcanic Zone (NVZ) with 5 volcanic systems, Reykjanes Volcanic Zone (RVZ) with 3 volcanic systems, and the East Volcanic Zone (EVZ) with 8 volcanic systems. Large scale, linear volcanic belts and ridges include the Mid Icelandic Belt (MIB) with 2 volcanic systems, the Öræfajökull Volcanic Belt (ÖVB) with 3 volcanic systems, and the Snæfellsnes Volcanic Belt (SVB) which also contains 3 volcanic systems (Thordarson and Larsen, 2007).

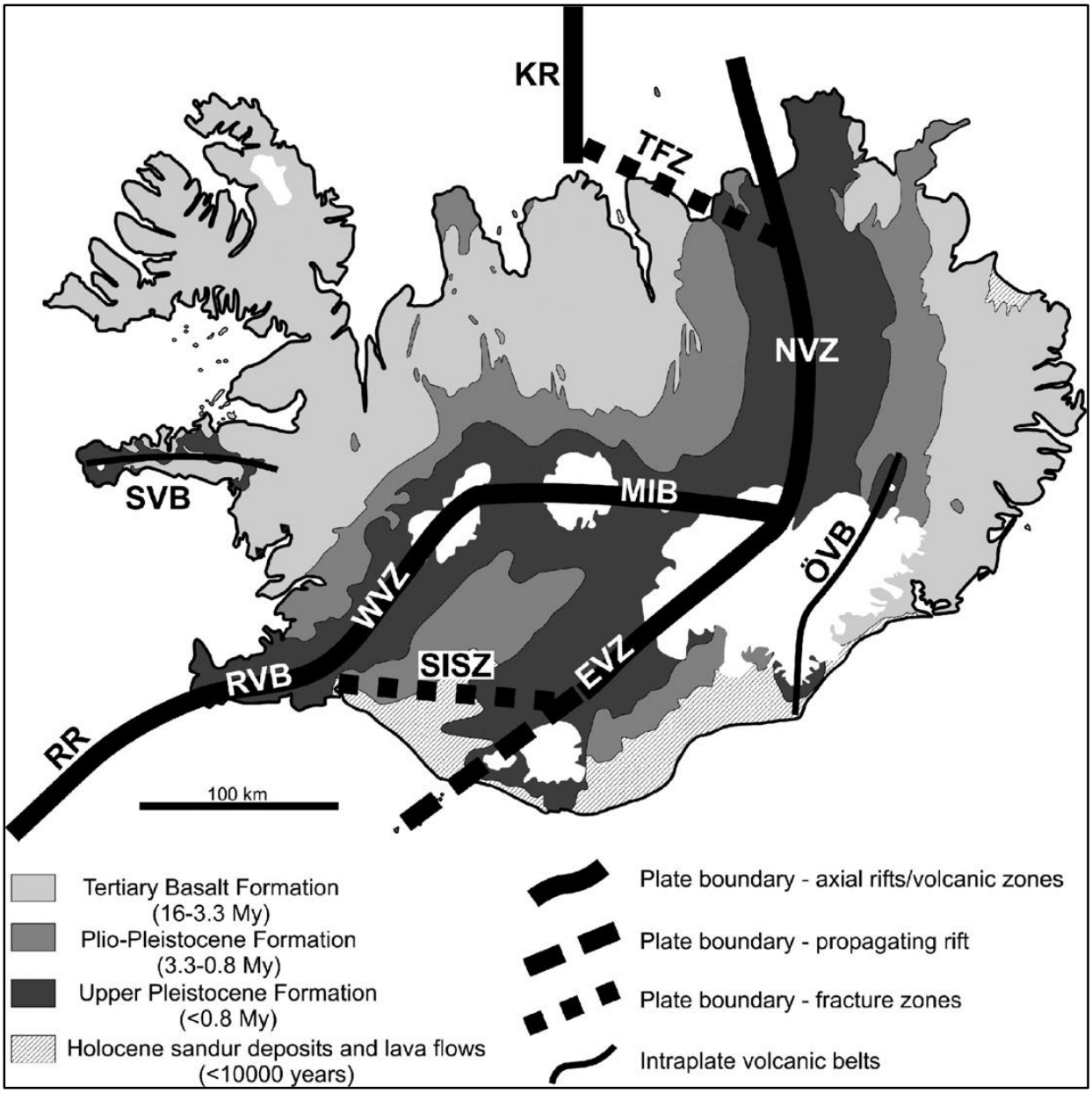


**Figure 7**: The general geology of Iceland, including the positions of plate boundaries, axial rifts, volcanic belts, and volcanic zones. RR, Reykjanes Ridge; RVB, Reykjanes Volcanic Belt; SISZ South Icelandic Seismic Zone; WVZ, West Volcanic Zone; MIB, Mid-Icelandic Belt; EVZ, East Volcanic Zone; NVZ, North Volcanic Zone; TFZ Tjörnes Fracture Zone; KR, Kolbeinsey Ridge; ÖVB, Öræfajökull Volcanic Belt; SVB, Snæfellsnes Volcanic Belt (Thordarson and Larsen, 2007).

The East Volcanic Zone is the region with the most active volcanism, in which about 80% of volcanic eruptions occur. The remaining 25% are distributed between the West Volcanic Zone (9%), North Volcanic Zone (5%), Öræfajökull Volcanic Belt (1%), and Snæfellsnes Volcanic Belt (0.5%). The source volcano is unknown for about 4.5% of all known eruptions (Thordarson and Larsen, 2007). The 4 most active volcanic systems in the EVZ are Grímsvötn, Bárdarbunga–Veidivötn, Hekla, and Katla. The EVZ is located to the East of the Mid-Atlantic Ridge, and is therefore propagating towards the southwest of Iceland.

Icelandic volcanism is particularly complex for its location due to its unique geological conditions. It contains almost all of the main types of volcanoes, except the diatremes, which are essentially volcanic pipes associated with rapid gaseous expansion and explosion (Thordarson and Larsen, 2007). There is a large spectrum of erupted lava compositions, from mafic lava shields to felsic stratovolcanoes. Volcanic activity ranges from phreatomagmatic activity, which produces pyroclastic debris due to water-magma interaction, to effusive activity, in which the low viscosity magma pours across the ground. Volcanic environments include subaerial, subglacial, and submarine (Thordarson and Larsen, 2007). The latter two are responsible for high degrees of undercooling and quench crystallization of lava that can create pillow basalts and volcanic glass inclusions. Analysis of these glasses, along with coexisting olivine, is essential in order to determine the oxygen fugacity of the melt. Most of the eruptions on Iceland are effusive basalt; however there are ranges of explosive eruption styles. Mafic subglacial phreatomagmatic eruptions can be relatively violent. The more uncommon high viscosity, felsic eruptions can also have subplinian and plinian intensities, similar to the 79 A.D. eruption of Mt. Vesuvius, as observed and recorded by Pliny the Younger.

Characteristics of the various volcanic systems are determined by their composition and their particular tectonic setting. These volcanotectonic systems include fissure swarms or dyke swarms, which nearly parallel the axes of the volcanic zones. Of the 30 volcanic systems, 20 are fissure swarms. Of these 20, 12 are relatively well developed, 5 are intermediately developed, and 4 are beginning to develop in an embryonic stage (Thordarson and Larsen, 2007). The volcanotectonic systems of Iceland also include central volcanoes. These are typically the epicenter of volcanic activity and volcanic eruption, creating the more macroscopic topographical features. There are 23 central volcanoes in total located within 19 volcanic systems (Thordarson and Larsen, 2007). Some volcanic systems have a combination of central volcanoes and fissure swarms, known as “Vulkanbælter”, or volcanic belts.

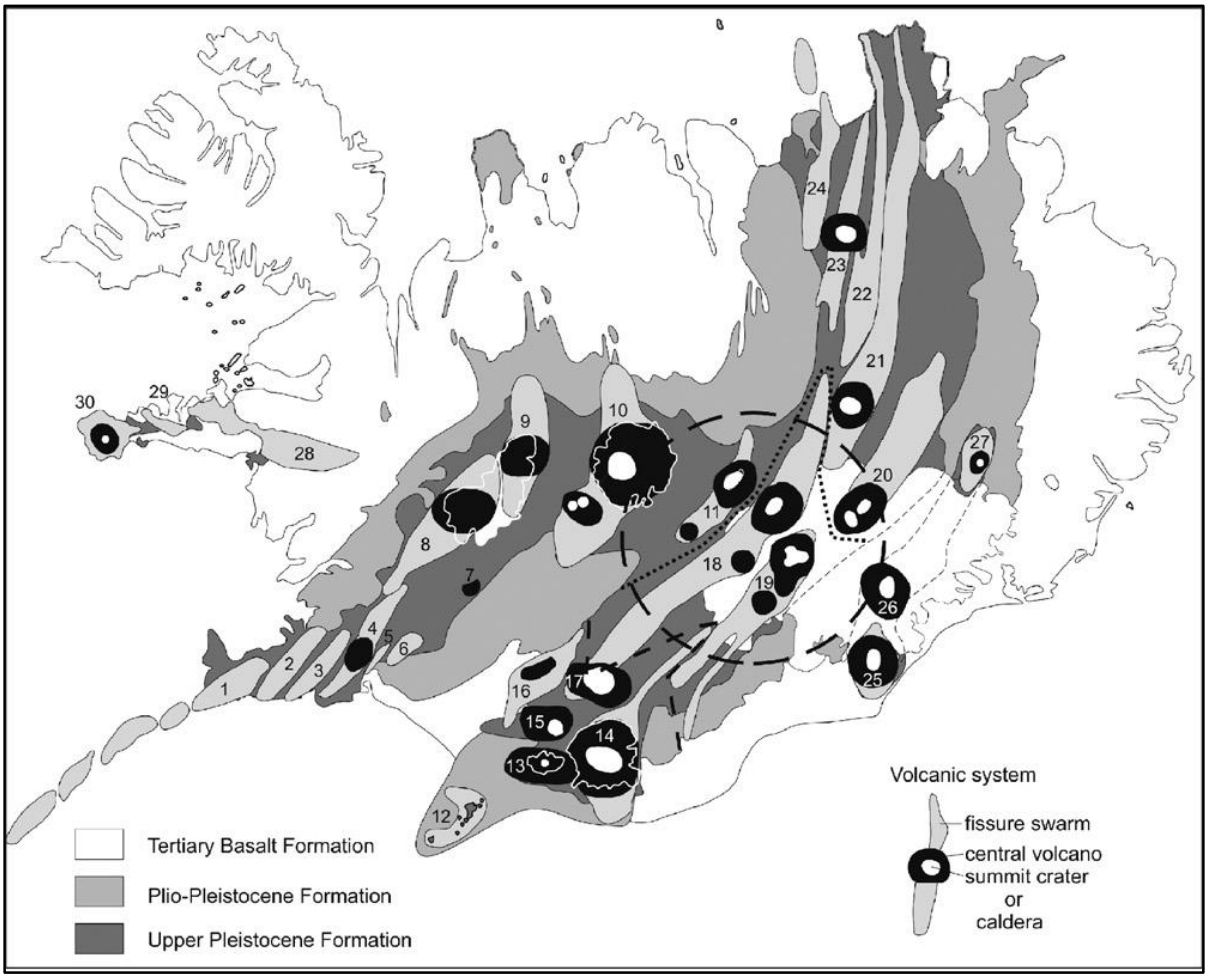


**Figure 8**: Distribution of active volcanic systems, as well as the shape of the fissure swarms, among volcanic zones and belts in Iceland as depicted by Jóhannesson and Sæmundsson (1998), from Thordarson and Larsen (2007). Reykjanes Volcanic Zone: (1) Reykjanes–Svartsengi, (2) Krýsuvík, (3) Brennisteinsfjöll; West Volcanic Zone: (4) Hengill, (5) Hrómundartindur, (6) Grímsnes, (7) Geysir, (8) Prestahnjúkur, (9) Langjökull; Mid-Iceland Belt: (10) Hofsjökull, (11) Tungnafellsjökull; East Volcanic Zone: (12) Vestmannaeyjar, (13) Eyjafjallajökull, (14) Katla, (15) Tindfjöll, (16) Hekla–Vatnafjöll, (17) Torfajökull, (18) Bárðarbunga–Veiðivötn, (19) Grímsvötn; North Volcanic Zone: (20) Kverkfjöll, (21) Askja, (22) Fremrinámur, (23) Krafla, (24) Þeistareykir; Öræfajökull Volcanic Belt: (25) Öræfajökull, (26) Esjufjöll, (27) Snæfell; Snæfellsnes Volcanic Belt: (28) Ljósufjöll, (29) Helgrindur, (30) Snæfellsjökull. The dashed circle represents an approximation of the center of the mantle plume. The black dotted line shows the northern boundary of the East volcanic Zone and the grey dashed line shows the boundary between the active and propagating rift segments.

Volcanic systems in Iceland

| | Volcanic zone | Name | Max. elev.[a] (m.a.s.l.) | Length (km) | Width (km) | Area ($km^2$) | Fissure swarm[b] | Central volcano[c] | Name of central volcano |
|---|---|---|---|---|---|---|---|---|---|
| 1 | RVZ | Reykjanes/Svartsengi | 163 | 58 | 13 | 350 | xxx | d | |
| 2 | RVZ | Krýsuvík | 393 | 55 | 13 | 300 | xxx | d | |
| 3 | RVZ | Brennisteinsfjöll | 621 | 45 | 10 | 280 | xxx | d | |
| 4 | WVZ | Hengill | 803 | 60 | 9 | 370 | xxx | cv | Hengill |
| 5 | WVZ | Hrómundartindur | 283 | 7 | 8 | 25 | | d | |
| 6 | WVZ | Grímsnes | 214 | 15 | 8 | 100 | xx | d | |
| 7 | WVZ | Geysir[c] | 600 | 7 | 7 | 25 | | d | |
| 8 | WVZ | Prestahnjúkur | 1400 | 80 | 27 | 950 | xxx | cv | Prestahnjúkur |
| 9 | WVZ | Hveravellir | 1000 | 60 | 18 | 720 | xx | cv | Hveravellir |
| 10 | MIB | Hofsjökull | 1800 | 95 | 38 | 2200 | xxx | cv | Hofsjökull/Kerlingarfjöll |
| 11 | MIB | Tungnafellsjökull | 1520 | 55 | 15 | 530 | xx | cv | Tungnafellsjökull/Hágöngur |
| 12 | EVZ | Vestmannaeyjar | 283 | 28 | 25 | <480 | xx | d | |
| 13 | EVZ | Eyjafjallajökull | 1666 | 30 | 14 | 300 | | cv | Eyjafjallajökull |
| 14 | EVZ | Katla | 1480 | 110 | 30 | 1300 | x | cv | Mýrdalsjökull |
| 15 | EVZ | Tindfjöll[c] | 1462 | 20 | 14 | 230 | | cv | Tindfjöll |
| 16 | EVZ | Hekla-Vatnafjöll | 1491 | 60 | 19 | 720 | xx | cv | Hekla |
| 17 | EVZ | Torfajökull | 1278 | 50 | 20 | 900 | | cv | Torfajökull |
| 18 | EVZ | Bárdarbunga-Veidivötn | 2009 | 190 | 28 | 2500 | xxx | cv | Bárdarbunga/Hamarinn |
| 19 | EVZ | Grímsvötn | 1722 | 100 | 23 | 1350 | x | cv | Grímsvötn/Thórdarhyrna |
| 20 | NVZ | Kverkfjöll | 1934 | 120 | 20 | 1600 | xxx | cv | Kverkfjöll |
| 21 | NVZ | Askja | 1510 | 200 | 20 | 2300 | xxx | cv | Askja |
| 22 | NVZ | Fremrinámur | 800 | 150 | 15 | 1200 | xxx | d | |
| 23 | NVZ | Krafla | 818 | 100 | 19 | 900 | xxx | cv | Krafla |
| 24 | NVZ | Theistareykir | 600 | 90 | 9 | 650 | xxx | d | |
| 25 | ÖVB | Öræfajökull | 2110 | 20 | 21 | 250 | | cv | Öræfajökull |
| 26 | ÖVB | Esjufjöll[d] | 1760 | 25 | 21 | 400 | | cv | Snæhetta |
| 27 | ÖVB | Snæfell[d] | 1833 | 20 | 11 | 170 | | cv | Snæfell |
| 28 | SVB | Ljósufjöll | 1063 | 80 | 15 | 720 | x | d | |
| 29 | SVB | Helgrindur (Lýsuskard) | 647 | 30 | 8 | 220 | x | d | |
| 30 | SVB | Snæfellsjökull | 1446 | 30 | 20 | 470 | | cv | Snæfellsjökull |

Based on Jóhannesson and Sæmundsson (1998).
[a] Maximum elevation above sea level.
[b] xxx, mature; xx, moderate maturity; x, embryonic.
[c] cv, central volcano; d, domain.
[d] No verified eruption of Holocene age.

**Table 1**: Information of the volcanic systems of Iceland. The numbers to the left coincide with the Figure 8. This table provides information regarding the size and dimension of each system, the maturity of the fissure swarm, as well as the name of the central volcano if one is present (Thordarson and Larsen, 2007).

There are 2 models for subsurface structure of the magma plumbing systems and how it affects the volcanic systems of Iceland during primary rifting incidents (Thordarson and Larsen, 2007). Each model contrasts the other in terms of depth of the magma chamber. The first model hypothesizes that a shallow crustal chamber injects dykes into the fissure swarm, which induces rifting. Another model hypothesizes that a deep, 20 km, magma chamber at the base of the crust

injects dykes into the fissure swarm, which causes rifting. Kelley and Barton (2008) have calculated pressures of crystallization from basalt glasses. There was a wide range of calculated pressures, between .001 and 1 GPa (indicating depths between 0 and 35 km). This suggests a relatively deep magma chamber close to the Mohorovičić discontinuity, where magma tends to pool at the boundary between the crust and the mantle. According to Kelley and Barton (2008), magma evolution is complex, and may involve multiple stacked magma chambers. Icelandic magma likely undergoes the process of polybaric crystallization, mixing, and assimilation en route to the surface (Kelley and Barton, 2008).

### *3.2 FAMOUS Region*

Samples from the FAMOUS region of the Mid-Atlantic Ridge were also analyzed in order to determine the oxygen fugacity of the mantle source regions. This location was chosen because it is relatively well sampled and contains many olivine-hosted melt inclusions, which are primary targets for the application of the olivine-melt equilibrium method for determining oxygen fugacity. Many fresh basalt samples were collected by the submersible *Alvin* during the FAMOUS (French American Mid-Ocean Undersea Study) project between 1973 and 1974. More samples were retrieved by dredging and core sampling from surface ships during this time. Most samples are related to distinctive topographical or geological submarine features, which were located by acoustic navigation systems (Bryan and Moore, 1977). These features were selected in order to collect samples of the most recent fresh lava flows. These samples are likely to contain fresh, unaltered volcanic glass. The FAMOUS region is located on the Mid-Atlantic Ridge at 37°47’N latitude on the ridge. The ridge segment is approximately 45 km long, and is bounded on the north and south by offsets of 25 km (Laubier et al., 2012). The northern

displacement is known as the North FAMOUS segment, and the southern displacement is the AMAR segment.

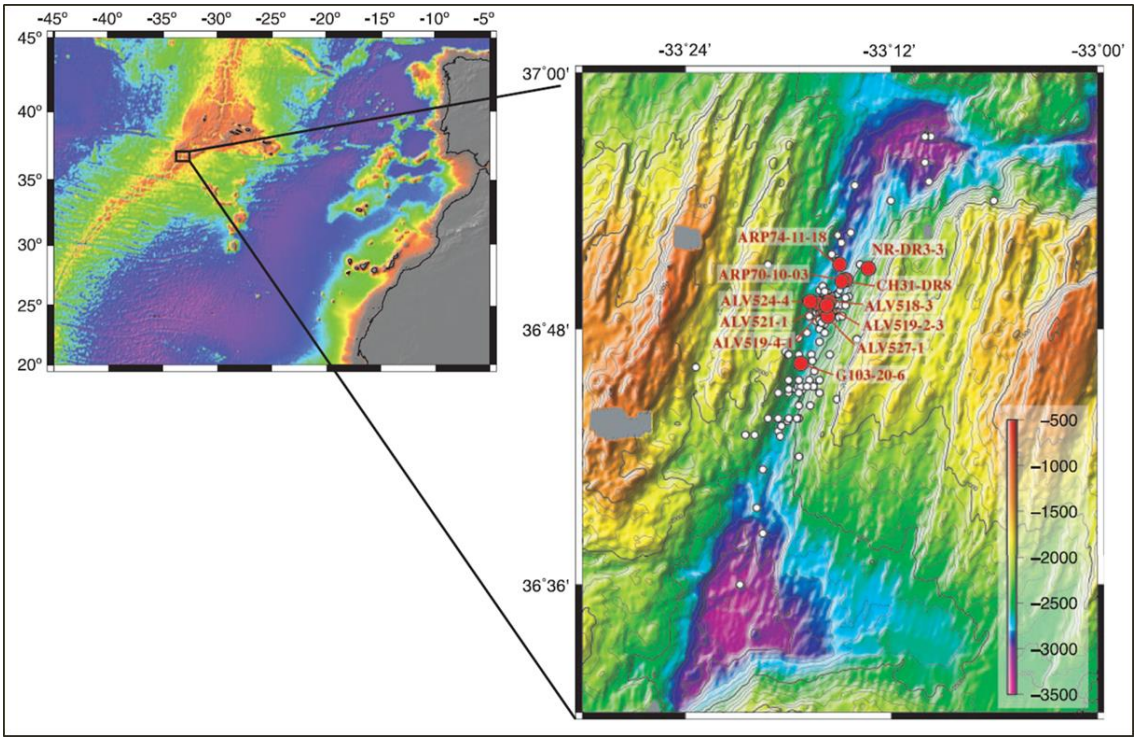


**Figure 9:** Bathymetric map of the FAMOUS region of the Mid-Atlantic Ridge, showing the locations of the melt inclusion samples (red circles) and glass samples (white circles) from the dataset from Laubier et al. (2012).

The central valley of the FAMOUS area contains normal faults due to the extensional stresses, which are believed to be somewhat listric and steepen downwards as seen in Figure (10) (Bryan and Moore, 1977). The dikes at the axis of the FAMOUS segment are slightly asymmetrical, likely due to the asymmetry in spreading rates. The central dikes are near vertical and tap into more primitive melts, whereas the marginal dikes are dipping towards the central axis and tap into more differentiated melts (Bryan and Moore, 1977). The FAMOUS region has a

relatively slow, asymmetric spreading rate for Mid-Ocean Ridges, at 0.7 cm/yr to the west and 1.5 cm/yr to the east (Bryan and Moore, 1977). This slow spreading rate may cause intermittent blocking of the volcanic vents when lava accumulates or when the walls of the vents collapse. These phenomena could halt eruptions, which explain the gaps in time recorded by the ages of the lava flows on the central valley of the FAMOUS region (Bryan and Moore, 1977).

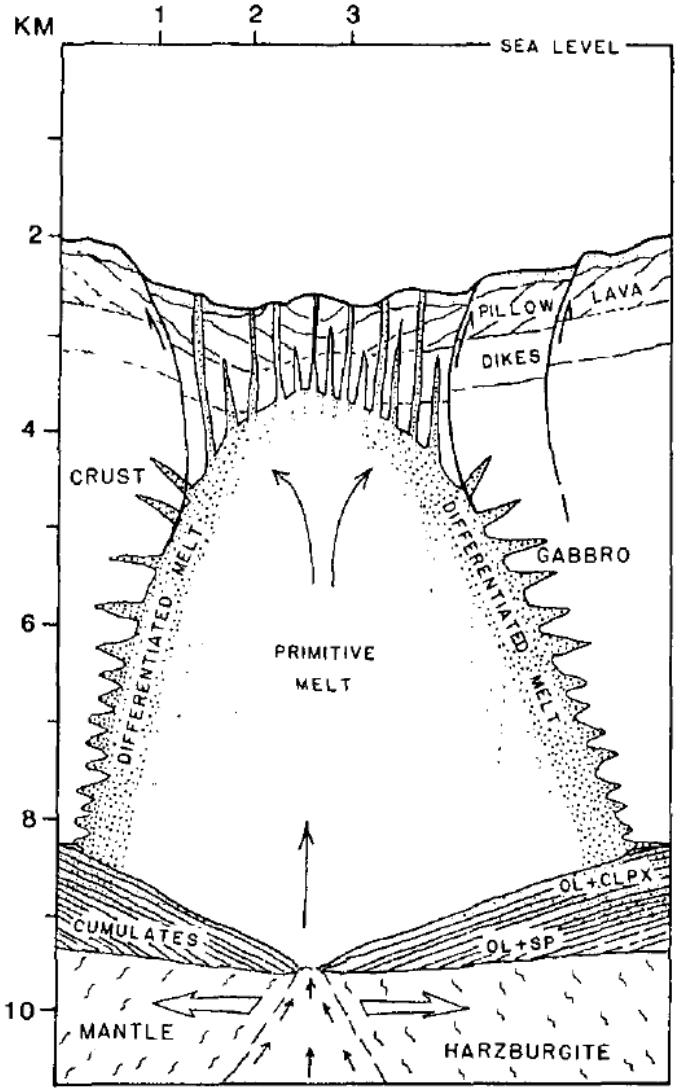


**Figure 10:** Model of inferred magma chamber of the median valley of the FAMOUS region. This model shows the position of the faults and dikes, showing the asymmetry of the chamber. Stipple indicates the differentiated melt in the magma chamber, including cumulates and lavas generated from it (Bryan and Moore, 1977).

# 4. Results

### *4.1 Iceland Results*

Oxygen fugacities were calculated for 67 samples from several different localities in Iceland, including: Borgarhraun, Búrfell, Einstæðingur, Fontur, Gaesafjoll, Giglodur, Herðubreiðartogl, Hrimalda, Kistufell, Mælifell, Miðfell, Reykjanes Ridge, Saxi, Seljahall, and Stapafell. Datasets were retrieved from published research articles, including Breddam (2002), and Thomson and Maclennan (2013); as well as datasets from PetDB (described by Lehnert et al. (2000)) and Geomapapp (described by Ryan et al. (2009)). Many samples are from Iceland's East Volcanic Zone because it is the most volcanically active and yields fresh, unaltered volcanic glass. The average oxygen fugacity calculated for these samples is -0.637 log units relative to the FMQ buffer.

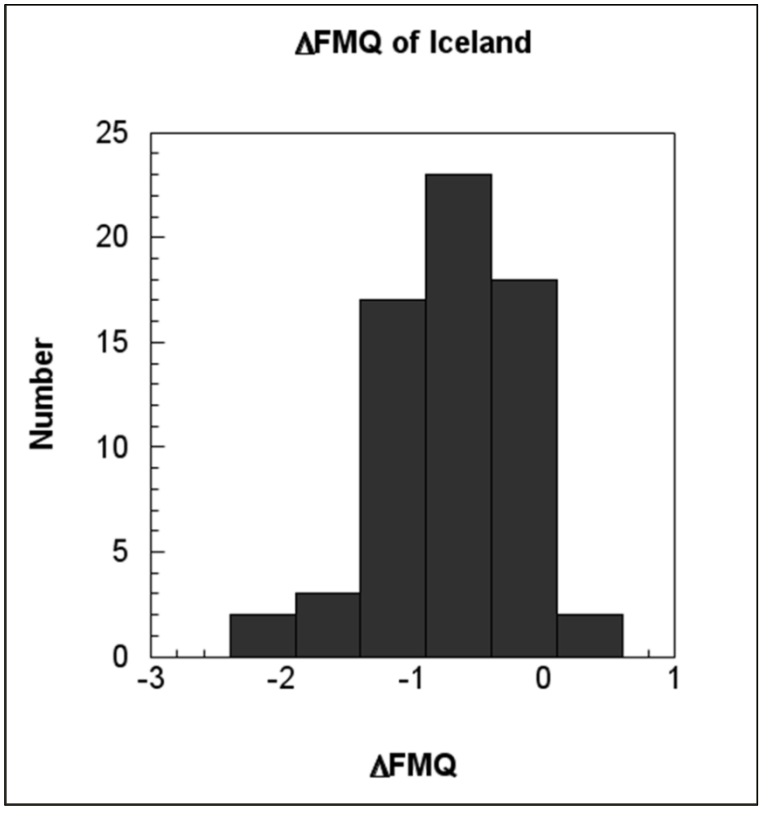


**Figure 11:** Histogram of the oxygen fugacities of Iceland relative to the FMQ buffer plotted against the number of occurrences (n = 67).

| Iceland | **Fo** | **Mg#** | **$K_D$** | **$K_D$** | **log $fO_2$** | **ΔFMQ** |
|---|---|---|---|---|---|---|
| Minimum: | 0.62 | 0.313 | 0.26 | 0.32 | -10.5 | -2.18 |
| Maximum: | 0.886 | 0.678 | 0.3 | 0.33 | -7.15 | 0.66 |
| Average: | 0.828 | 0.581 | 0.28 | 0.32 | -8.9 | -0.64 |

**Table 2**: Summary of the dataset from Iceland showing forsterite mole percent, Mg# of the liquid (MgO/MgO+FeO), the distribution coefficients (first with all iron reported as FeO, second calculated with ferric and ferrous iron), log $fO_2$, and deviation in $fO_2$ from the FMQ buffer in log bar units.

### *4.2 FAMOUS Region Results*

Oxygen fugacities for the FAMOUS region of the Mid-Atlantic Ridge were calculated primarily using the large dataset from Laubier et al. (2012). The dataset is composed of 316 melt inclusions from 14 different rock samples taken along the axis of the FAMOUS region. The average oxygen fugacity calculated for this region is equal to -1.63 log units relative to the FMQ buffer.

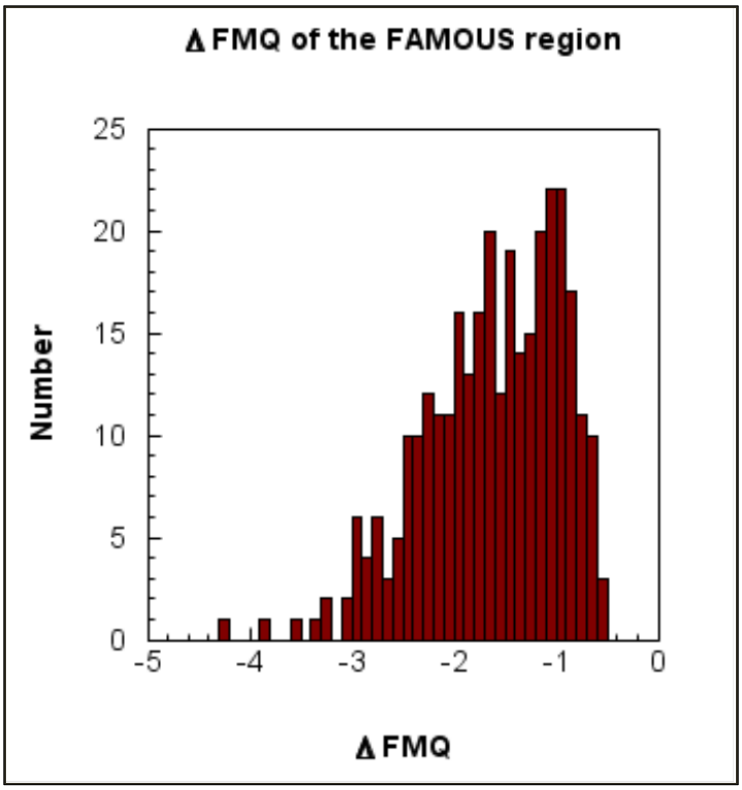


**Figure 12:** Histogram of the oxygen fugacities of the FAMOUS region of the Mid-Atlantic Ridge relative to the FMQ buffer plotted against the number of occurrences (n = 316).

| | **Fo** | **Mg#** | **$K_D$** | **$K_D$** | **log $fO_2$** | **ΔFMQ** |
|---|---|---|---|---|---|---|
| Minimum: | 0.853 | 0.638 | 0.28 | 0.31 | -10.8 | -4.3 |
| Maximum: | 0.922 | 0.78 | 0.3 | 0.33 | -7.88 | -0.55 |
| Average: | 0.893 | 0.711 | 0.29 | 0.32 | -9.06 | -1.63 |

**Table 3:** Summary of the dataset from the FAMOUS region showing forsterite mole percent, Mg# of the liquid (MgO/MgO+FeO), the distribution coefficients (first with all iron reported as FeO, second calculated with both ferric and ferrous iron), log $fO_2$, and deviation in $fO_2$ from the FMQ buffer in log bar units.

# 5. Discussion

Uncertainties in establishing equilibrium for olivine-melt pairs arise when considering whether or not a particular olivine-melt pair represents equilibrium conditions. As a first approximation, if the calculated distribution coefficient does not fall within the range of $0.3 \pm 0.03$, then the olivine did not equilibrate from the particular melt being analyzed, and it is likely a xenocryst (Roeder and Emslie, 1970). This approach has been frequently used to determine whether a particular olivine-melt pair from published data represents equilibrium conditions or not.

Selecting the correct olivine for this procedure can be a difficult task. If several forsterite mole percentages are reported on a zoned crystal, it is necessary to construct zoning profiles in order to identify probable equilibrium olivine compositions. During the process of selection, it appears that microphenocrysts or olivine phenocryst rims give the best results (and yield appropriate values for the distribution coefficient). This sometimes poses a problem with data selection when using published data, because many researchers analyze only the olivine macrocrysts, which are typically not in equilibrium with the melt. In other cases, the precise location in the crystal that was analyzed (e.g. core or rim) is not specified. In many cases, there are no olivine-melt pairs, only volcanic glass analyses. In such cases, the datasets are not designed to study the partitioning of ferrous iron and magnesium between the olivine and melt. Therefore, the most beneficial datasets are those that include multiple analyses of olivine melt pairs that provide insight into rim to core compositional profiles. Volcanic glass in the form of melt inclusions inside olivine phenocrysts are the primary targets for the application of the olivine-melt method. These tend to give the most consistent results.

Anomalous samples for which calculated values of $K_D$ markedly deviate from the ideal value are rare but any that occurred have been discarded. These samples include those that are specifically mentioned by the author of the article from which the dataset was extracted. If a particular sample from the dataset is significantly different from the others, then there may be analytical errors affecting the olivine and glass compositional data. There is likely a problem with the sample if it does not have acceptable stoichiometry of olivine.

# 6. Conclusions

The calculated oxygen fugacities for both Iceland and the FAMOUS region of the Mid-Atlantic Ridge yielded results that are comparable with other calculated oxygen fugacities from Mid-Ocean Ridge Basalts in general. The results obtained from this research using the olivine-melt equilibrium method were consistent with other methods used in order to determine oxygen fugacity of mantle source regions. Figure (13) shows the comparison with other methods used to calculate oxygen fugacity, such as the QUILF method and directly using the ferric to ferrous iron ratios. The results for Iceland and Mid-Ocean Ridge Basalts yield similar numbers, close to -1 log units below the FMQ buffer.

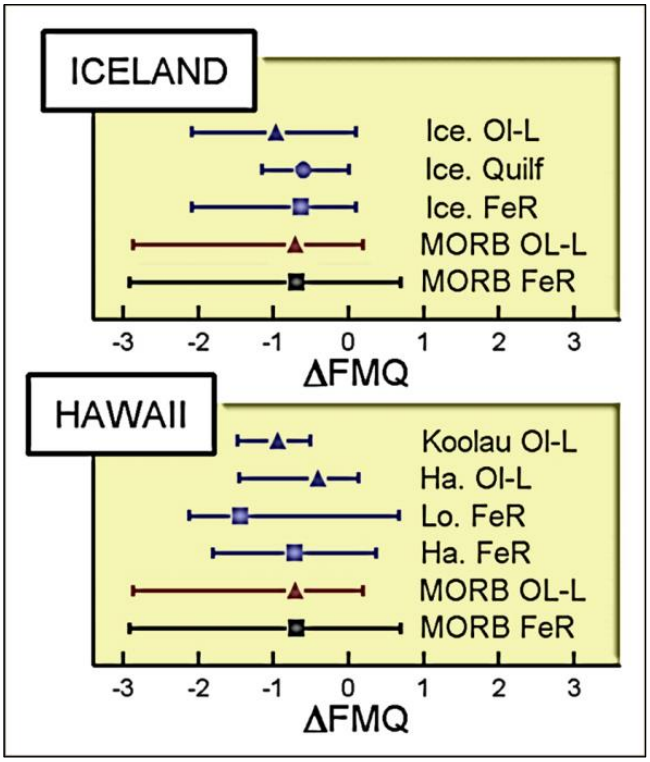


**Figure 13:** Distribution of oxygen fugacities relative to the FMQ buffer using different methods, including: The Olivine-Melt Equilibrium method (Ol-L), the Quartz-Ulvöspinel-Ilmenite-Fayalite method (QUILF), and the direct ferric to ferrous iron ratio method (FeR). Locations include Iceland and Hawaii, which are compared with Mid-Ocean Ridge Basalts (MORB) (Barton, unpublished data).

These results support the hypothesis that the olivine-melt equilibrium method can be used to determine oxygen fugacity. There are some difficulties with establishing a correct olivine-melt pair that truly represents equilibrium conditions. However, this method does have its advantages, such as exploiting the abundance of olivine in igneous rocks. It is also advantageous that both the ferric and ferrous iron contents of the melt are not required because they can be indirectly calculated. This process only requires common instrumentation, such as an electron microprobe, as opposed to rare and expensive instrumentation, such as a synchrotron. This could potentially benefit many geochemists and igneous petrologists by providing a useful new method in order to determine the redox state of magma and its mantle source regions.

# 7. Future Work

Future directions for this research include applying the olivine-melt equilibrium method to other Mid-Ocean Ridge Basalts, such as the East Pacific Rise between the Siqueiros and Clippterton Fracture Zones. Ocean Island Basalts can also be analyzed, including the Galapagos Islands, the Canary Islands, and Hawaii. It is also possible to apply this method to volcanic arcs, as long as they contain sufficient olivine phenocrysts and melt inclusions.

Once sufficient numbers are calculated for these various locations with different tectonic environments, information regarding the redox state of the mantle can be established. This information can be used to monitor global variations in oxygen fugacity in Earth's mantle. Attempts can then be made in order to address the question of what is petrologically influencing the variation in oxygen fugacity around the world.

If there are sufficient datasets, it would be possible to calculate how the oxygen fugacity of a source has changed through geologic time. Calculating ancient oxygen fugacities poses a problem because volcanic glass is very susceptible to chemical weathering and devitrification, therefore older samples containing fresh volcanic glass are more difficult to acquire and analyze. If Archean samples could be analyzed, this method could be used to determine when the oxidation state of the mantle has increased as a response to the onset of plate tectonics. At some time in the Archean, the Earth differentiated enough to form a solid crust, which eventually subducted, initiating plate tectonics. The process of subduction introduces water into Earth's mantle, which would drastically affect its redox state. The question of when plate tectonics began on Earth is still a matter of controversy; however this method could be used to form a valid hypothesis of the onset of plate tectonics. The presence of fresh olivines and glasses in samples

of Archean Komatiites recovered from drill cores offers promise for studies of potential changes in the redox state of the earth's interior through time.

As many oxygen fugacities are calculated for different locations, it is beneficial to continue to test this method and attempt to analyze what exactly influences the distribution coefficient. Compositional influences on the distribution coefficient should be observed, such as the influence of aluminum and alkalis, which suggests crustal interactions and anatexis. It is also essential to constrain how other factors, such as degassing and crystallization, impact oxygen fugacity.

# 8. References


Anderson, D.J., Bishop, F.C., and Lindsley, D.H., 1991, Internally consistent solution models for Fe-Mg-Mn-Ti oxides; Part II. Fe-Mg-Ti oxides and olivine: Am. Min., v. 76, p. 427-444.

Anderson, D.J., and Lindsley, D.H., 1988, Internally consistent solution models for Fe-Mg-Mn-Ti oxides; Fe-Ti oxides: Am. Min., v. 73, p. 714-726.

Ballhaus, C.G., Berry, R.F., Green, D.H., 1990, Oxygen fugacity controls in the Earth's upper mantle: Nature, v. 348, p. 437-440.

Ballhaus, C.G., Berry, R.F., Green, D.H., 1991, High pressure experimental calibration of the olivine-orthopyroxene-spinel oxygen geobarometer; implications for the oxidation state of the upper mantle: Contrib. Mineral. Petrol., v. 107, p. 27-40.

Barton, M., 2003, Composition of olivine, melt redox state, and oxygen fugacity: Eos, Transactions of the American Geophysical Union, 84, F1584

Bézos, A., and Humler, E., 2005, The Fe3+/ΣFe ratios of MORB glasses and their implications for mantle melting: Geochim. Cosmochim. Acta, v. 69, p. 711-725.

Bowen, N.L., and Schairer, J.F., 1935, The System MgO-FeO-SiO2: American Journal of Science, v. 29, p. 151-217

Bown, J.W., and White, R.S., 1994, Variation with Spreading Rate of Oceanic Crustal Thickness and Geochemistry: Earth and Planetary Science Letters, v. 121, p. 435-449.

Breddam, K., 2002, Kistufell: Primitive Melt from the Iceland Mantle Plume: Journal of Petrology, v. 43.2, p. 345.

Bryan, W.B., and Moore, J.G., 1977, Compositional Variations of Young Basalts in the Mid-Atlantic Ridge Rift Valley Near Lat 36°49′N: Geological Society of America Bulletin, v. 88.4.

Buddington, A.F., and Lindsley, D.H., 1964, Iron-titanium oxide minerals and synthetic equivalents: J. Petrol., v. 5, p. 310-357.

Carmichael, I.S.E., 1991, The Redox States of Basic and Silicic Magmas: a Reflection of Their Source Regions?: Contributions to Mineralogy and Petrology, v. 106.2, p. 129-141.

Carmichael, I.S.E., and Ghiorso, M.S., 1986, Oxidation-reduction Relations in Basic Magma: a Case for Homogeneous Equilibria: Earth and Planetary Science Letters, v. 78, p. 200-210.

Carmichael, I.S.E., and Ghiorso, M.S., 1990, The effect of oxygen fugacity on the redox state of natural liquids and their crystallizing phases: Rev. Mineral., v. 24, p. 191-212.

Christie, D.M., Charmichael, I.S.E., and Langmuir, C.H., 1986, Oxidation states of mid-ocean ridge basalt glasses: Earth Planet. Sci. Lett., v. 79, p. 397-411.

Delaney, J.S., Bajt, S., Carmichael, I.S.E., Dyar, M.D., McKay, G, Moore, G., Roeder, P., and Sutton, S.R., 1996, In situ microanalysis of ferric/ferrous in geologically significant glasses: Abs. Prog. Geol. Soc. Am., v. 28, p. 419.

Eugster, H.P., 1957, Heterogeneous Reactions Involving Oxidation and Reduction at High Pressures and Temperatures: *The Journal of Chemical Physics*, v. 26.6, p. 1760.

Faure, G., 1998, Principles and Applications of Geochemistry: A Comprehensive Textbook for Geology Students: Upper Saddle River, N.J., Prentice Hall, p. 166-168.

Frost, B.R., Lindsley, D.H., and Andersen, D.J., 1988, Fe-Ti-oxide-silicate equilibria: assemblages with fayalitic olivine: Am. Mineral., v. 73, p. 727-740.

Frost, B.R., and Lindsley, D.H., 1992, Equilibria Among Fe-Ti Oxides, Pyroxenes, Olivine, and Quartz: Part II. Application: American Mineralogist, v. 77.9, p. 1004.

Gee, L.L., and Sack, R.O., 1988, Experimental Petrology of Melilite Nephelinites: Journal of Petrology, v. 29.6, p. 1233-1255.

Ghiorso, M.S., and Sack, R.O., 1991, Fe-Ti oxide geothermometry: thermodynamic formulation and estimation of intensive variables in silicic magmas: Contrib. Mineral. Petrol., v. 108, p. 485-510.

Jóhannesson, H., Sæmundsson, K., 1998, Geological Map of Iceland, 1:500,000: Bedrock Geology, Icelandic Institute of Natural History and Iceland, Geodetic Survey, Reykjavík.

Kelley, D.F. and Barton, M., 2008, Pressures of Crystallization of Icelandic Magmas: Journal of Petrology, v. 49.3, p. 465-492.

Kilinc, A., Carmichael, I.S.E., Rivers, M.L., and Sack, R.O., 1983, The Ferric-Ferrous Ratio of Natural Silicate Liquids Equilibrated in Air: Contributions to Mineralogy and Petrology, v. 83, p. 136-140.

Kress, V.C., and Carmichael, I.S.E., 1991, The Compressibility of Silicate Liquids Containing Fe2O3 and the Effect of Composition, Temperature, Oxygen Fugacity and Pressure on Their Redox States: Contributions to Mineralogy and Petrology, v. 108, p. 82-92.

Laubier, M, Gale, A and Langmuir, C.H., 2012, Melting and Crustal Processes at the Famous Segment (Mid-Atlantic Ridge): New Insights from Olivine-Hosted Melt Inclusions from Multiple Samples: Journal of Petrology, v. 53.4, p. 665-698.

Leftwich, T.E., von Frese, R.B., Potts, L.V., Kim, H.R., Roman, D.R., Taylor, P.T., and Barton, M., 2005, Crustal modeling of the North Atlantic from spectrally correlated free-air and terrain gravity: Journal of Geodynamics, v. 40, p. 23-50.

Lehnert, K., Su, Y., Langmuir, C., Sarbas, B., and Nohl, U., 2000, A global geochemical database structure for rocks: Geochem. Geophys. Geosyst. 1, doi:10.1029/1999GC000026

Lewis, G.N., 1901, The Law of Physico-Chemical Change: Proceedings of the American Academy of Arts and Sciences, v.37, p. 49–69.

Lindsley, D.H., 1991, Oxide Minerals: Petrologic and Magnetic Significance, *in* Lindsley, D.H., ed., Experimental Studies of Oxide Minerals: Washington, D.C, Reviews in Mineralogy, v. 25, p. 69-106.

Lindsley, D.H, Frost, B.R., Andersen, D.J., and, Davidson, P.M., 1990, Fe-Ti oxide-silicate equilibria: Assemblages with orthopyroxene. In R.J. Spencer and I.M. Chou, Eds., Fluid-mineral interactions: A tribute to H.P. Eugster, special publication v. 2, p. 103-119.

Lindsley, D.H., and Frost, B.R., 1992, Equilibria Among Fe-Ti Oxides, Pyroxenes, Olivine, and Quartz: Part I. Theory: American Mineralogist, v. 77.9, p. 987.

Longhi, J., Walker, D., Hays, J.F., 1978, The Distribution of Fe and Mg between Olivine and Lunar Basaltic Liquids: Geochimica et Cosmochimica Acta, v. 42, p. 1545-1558.

Miller, E.D., Kelley, D.F., and Barton, M., 2005, Mg-$Fe^{2+}$ exchange between olivine and melt, EOS Trans. AGU, 86(18), Joint Assem. Suppl., Abstract V13B-08.

Nordstrom, D.K., and Munoz, J.L., 1994, Geochemical Thermodynamics: Boston, Blackwell Scientific Publications, p. 129-131, p. 305-317.

Passmore, E., Fitton, G., Thordarson, T., and Maclennan, J., 2012, Mush Disaggregation in Basaltic Magma Chambers: Evidence from the Ad 1783 Laki Eruption: Journal of Petrology, v. 53.12, p. 2593-2623.

Philpotts, A.R., and Ague J.J., 2009, Principles of Igneous and Metamorphic Petrology: Cambridge, UK, Cambridge University Press, p. 243-265.

Roeder, P.L., and Emslie, R.F., 1970, Olivine-liquid Equilibrium: Contributions to Mineralogy and Petrology, v. 29.4, p. 275-289.

Ryan, W.B.F., Carbotte, S.M., Coplan, J.O., O'Hara, S., Melkonian, A., Arko, R., Weissel, R.A., Ferrini, V., Goodwillie, A., Nitsche, F., Bonczkowski, J., and Zemsky, R., 2009, Global Multi-Resolution Topography synthesis: Geochem. Geophys. Geosyst., 10, Q03014, doi:10.1029/2008GC002332.

Sugawara, T., 2000, Empirical relationships between temperature, pressure, and MgO content in olivine and pyroxene saturated liquid: Journal of Geophysical Research, B, Solid Earth and Planets, v. 105, p. 8457-8472.

Thomson, A., and Maclennan, J., 2013, The Distribution of Olivine Compositions in Icelandic Basalts and Picrites: Journal of Petrology, v. 54.4, p. 745-768.

Thordarson, T., and Larsen, G., 2007, Volcanism in Iceland in Historical Time: Volcano Types, Eruption Styles and Eruptive History: Journal of Geodynamics, v. 43.1, p. 118-152.

Toplis, M.J., 2005, The Thermodynamics of Iron and Magnesium Partitioning between Olivine and Liquid: Criteria for Assessing and Predicting Equilibrium in Natural and Experimental Systems: Contributions to Mineralogy and Petrology, v. 149.1.

# 9. Appendix

The following tables contain summarized data from Iceland and the FAMOUS region of the Mid-Atlantic Ridge. These data were retrieved from published research articles, including Thomson and Maclennan (2013) (reference #1), Breddam (2002) (reference #2), and Laubier et al. (2012) (reference #5). More data were retrieved from PetDB using Geomapapp (reference #3) and Barton, personal data (reference #4). The locations in which the Icelandic samples were retrieved is listed below, and the FAMOUS sample locations are displayed in Figure 9. The forsterite mole percent and Mg# of the liquid are reported, where Mg# is defined as MgO/(MgO+FeO). Two distribution coefficients are given, first with all iron reported as FeO, whereas the second is calculated with both ferric and ferrous iron. These samples were processed using the olivine-melt equilibrium method and the resulting log $fO_2$ and its deviation from the FMQ buffer in log bar units are also reported in this appendix. These datasets are available upon request.

### *9.1 Iceland*

| **Locality** | **Ref.** | **Sample #** | **Fo** | **Mg#** | **$K_D$** | **$K_D$** | **log $fO_2$** | **ΔFMQ** |
|---|---|---|---|---|---|---|---|---|
| Borgarhraun | 1 | ol1 | 0.86 | 0.624 | 0.27 | 0.32 | -8.07 | -0.02 |
| Borgarhraun | 1 | ol2 | 0.86 | 0.634 | 0.28 | 0.32 | -8.65 | -0.64 |
| Einstæðingur | 1 | Lit2_ol52_1 | 0.779 | 0.498 | 0.28 | 0.32 | -9.29 | -0.77 |
| Gaesafjoll | 1 | G01 | 0.805 | 0.53 | 0.27 | 0.32 | -8.54 | -0.16 |
| Gaesafjoll | 1 | G05 | 0.805 | 0.541 | 0.29 | 0.32 | -9.35 | -1.03 |
| Gaesafjoll | 1 | G06 | 0.805 | 0.546 | 0.29 | 0.32 | -9.76 | -1.46 |
| Gaesafjoll | 1 | G07 | 0.805 | 0.54 | 0.28 | 0.32 | -9.25 | -0.9 |
| Gaesafjoll | 1 | G08 | 0.805 | 0.542 | 0.29 | 0.32 | -9.46 | -1.12 |
| Gaesafjoll | 1 | G10 | 0.805 | 0.541 | 0.29 | 0.32 | -9.41 | -1.11 |
| Gaesafjoll | 1 | G12 | 0.805 | 0.545 | 0.29 | 0.32 | -9.71 | -1.42 |

| | | | | | | | | |
|---|---|---|---|---|---|---|---|---|
| Gaesafjoll | 1 | G13 | 0.805 | 0.54 | 0.28 | 0.32 | -9.24 | -0.91 |
| Gaesafjoll | 1 | G14 | 0.805 | 0.552 | 0.3 | 0.32 | -10.4 | -2.1 |
| Gaesafjoll | 1 | G15 | 0.805 | 0.536 | 0.28 | 0.32 | -8.91 | -0.53 |
| Gaesafjoll | 1 | G16 | 0.805 | 0.545 | 0.29 | 0.32 | -9.69 | -1.35 |
| Gaesafjoll | 1 | G17 | 0.805 | 0.551 | 0.3 | 0.32 | -10.5 | -2.18 |
| Gaesafjoll | 1 | G18 | 0.805 | 0.543 | 0.29 | 0.32 | -9.56 | -1.24 |
| Gaesafjoll | 1 | G19 | 0.805 | 0.541 | 0.29 | 0.32 | -9.4 | -1.08 |
| Gaesafjoll | 1 | GAE06u | 0.805 | 0.516 | 0.26 | 0.32 | -7.87 | 0.65 |
| Herðubreiðartogl | 1 | HBT10 1 | 0.866 | 0.651 | 0.29 | 0.32 | -9.06 | -1.22 |
| Herðubreiðartogl | 1 | HBT10 2 | 0.866 | 0.651 | 0.29 | 0.32 | -9.09 | -1.26 |
| Herðubreiðartogl | 1 | HT01 | 0.866 | 0.646 | 0.28 | 0.32 | -8.57 | -0.62 |
| Mælifell | 1 | 14052 | 0.855 | 0.629 | 0.29 | 0.32 | -9.19 | -1.11 |
| Mælifell | 1 | 14053 | 0.855 | 0.611 | 0.27 | 0.32 | -7.94 | 0.18 |
| Miðfell | 1 | 12459 | 0.865 | 0.634 | 0.27 | 0.32 | -7.94 | 0.07 |
| Midfell | 1 | MF01 | 0.865 | 0.646 | 0.29 | 0.32 | -10 | -1.14 |
| Stapafell | 1 | STAP_01 | 0.825 | 0.574 | 0.29 | 0.32 | -9.28 | -1.07 |
| Kistufell | 2 | nal594 | 0.867 | 0.645 | 0.28 | 0.32 | -8.58 | -0.62 |
| Kistufell | 2 | nal595 | 0.882 | 0.678 | 0.28 | 0.32 | -8.5 | -0.8 |
| Kistufell | 2 | nal596 | 0.871 | 0.653 | 0.28 | 0.32 | -8.59 | -0.67 |
| Kistufell | 2 | nal598 | 0.871 | 0.655 | 0.28 | 0.32 | -8.67 | -0.76 |
| Kistufell | 2 | nal606 | 0.865 | 0.635 | 0.27 | 0.32 | -8.16 | -0.17 |
| Kistufell | 2 | nal607 | 0.869 | 0.642 | 0.27 | 0.32 | -8.03 | -0.08 |
| Kistufell | 2 | nal609 | 0.866 | 0.65 | 0.29 | 0.32 | -9.18 | -1.31 |
| Kistufell | 2 | nal610 | 0.871 | 0.645 | 0.27 | 0.32 | -7.92 | -0.02 |
| Kistufell | 2 | nal611 | 0.88 | 0.653 | 0.26 | 0.32 | -7.15 | 0.66 |
| Reykjanes | 3 | TRI0101-012-006 | 0.724 | 0.441 | 0.3 | 0.33 | -10.2 | -1.36 |
| Reykjanes | 3 | TRI0101-027-001 | 0.851 | 0.602 | 0.26 | 0.33 | -7.58 | 0.59 |
| Reykjanes | 3 | TRI0101-033-006 | 0.825 | 0.58 | 0.29 | 0.33 | -9.25 | -0.97 |
| Reykjanes | 3 | TRI0101-034-006 | 0.813 | 0.558 | 0.29 | 0.33 | -9.06 | -0.72 |
| Fortur | 4 | FeR1 | 0.77 | 0.479 | 0.28 | 0.32 | -8.7 | -0.06 |
| Mælifell | 4 | FeR2 | 0.86 | 0.635 | 0.28 | 0.32 | -9.15 | -1.04 |

| | | | | | | | | |
|---|---|---|---|---|---|---|---|---|
| Búrfell | 4 | FeR3 | 0.62 | 0.313 | 0.28 | 0.33 | -9.28 | 0.07 |
| Mælifell | 4 | FeR4 | 0.865 | 0.635 | 0.27 | 0.32 | -8.4 | -0.3 |
| Mælifell | 4 | FeR5 | 0.875 | 0.66 | 0.28 | 0.32 | -8.44 | -0.53 |
| Mælifell | 4 | FeR6 | 0.875 | 0.66 | 0.28 | 0.32 | -8.5 | -0.55 |
| Mælifell | 4 | FeR7 | 0.886 | 0.676 | 0.27 | 0.32 | -7.74 | 0.09 |
| Mælifell | 4 | Glass inc1 | 0.875 | 0.658 | 0.27 | 0.32 | -8.25 | -0.34 |
| Mælifell | 4 | Glass inc2 | 0.885 | 0.676 | 0.27 | 0.32 | -8.16 | -0.29 |
| Iceland | 4 | FeR8 | 0.816 | 0.553 | 0.28 | 0.32 | -8.97 | -0.71 |
| Iceland | 4 | FeR9 | 0.808 | 0.541 | 0.28 | 0.32 | -9.03 | -0.62 |
| Fortur | 4 | FeR10 | 0.765 | 0.479 | 0.28 | 0.32 | -9.17 | -0.53 |
| Iceland | 4 | 2-7-12 | 0.801 | 0.529 | 0.28 | 0.32 | -9.06 | -0.6 |
| Seljahall | 4 | 30-6-2 | 0.794 | 0.518 | 0.28 | 0.32 | -8.93 | -0.54 |
| Halar | 4 | 9-7-7 | 0.822 | 0.562 | 0.28 | 0.32 | -8.6 | -0.33 |
| Iceland | 4 | 30-6-10 | 0.851 | 0.614 | 0.28 | 0.32 | -8.33 | -0.22 |
| Iceland | 4 | 338 | 0.836 | 0.586 | 0.28 | 0.32 | -8.68 | -0.51 |
| Iceland | 4 | 347 | 0.77 | 0.481 | 0.28 | 0.32 | -8.96 | -0.33 |
| Fortur | 4 | PARENT1 | 0.85 | 0.619 | 0.29 | 0.32 | -9.29 | -0.96 |
| Hrimalda | 4 | PARENT2 | 0.865 | 0.64 | 0.28 | 0.32 | -8.83 | -0.52 |
| Giglodur | 4 | PARENT3 | 0.87 | 0.646 | 0.27 | 0.32 | -8.35 | -0.18 |
| Fortur | 4 | FeR11 | 0.758 | 0.479 | 0.29 | 0.32 | -10.1 | -1.42 |
| Saxi | 4 | FeR12 | 0.758 | 0.463 | 0.28 | 0.32 | -8.84 | -0.09 |
| Saxi | 4 | FeR13 | 0.75 | 0.463 | 0.29 | 0.32 | -9.57 | -0.82 |
| Hrimalda | 4 | FeR14 | 0.84 | 0.591 | 0.27 | 0.32 | -8.72 | -0.44 |
| Hrimalda | 4 | FeR15 | 0.84 | 0.591 | 0.27 | 0.32 | -8.72 | -0.44 |
| Giglodur | 4 | FeR16 | 0.84 | 0.592 | 0.28 | 0.32 | -8.64 | -0.41 |
| Giglodur | 4 | FeR17 | 0.86 | 0.627 | 0.27 | 0.32 | -9.56 | -0.36 |

### *9.2 FAMOUS Region*

| Ref. | Sample # | Fo | Mg# | $K_D$ | $K_D$ | log $fO_2$ | ΔFMQ |
|---|---|---|---|---|---|---|---|
| 5 | ARP73-10-03-Ol1 | 0.897 | 0.721 | 0.3 | 0.32 | -9.21 | -1.94 |
| 5 | ARP73-10-03-Ol2 | 0.909 | 0.749 | 0.3 | 0.32 | -9.3 | -2.41 |
| 5 | ARP73-10-03-Ol3 | 0.902 | 0.733 | 0.3 | 0.32 | -9.2 | -2.1 |
| 5 | ARP73-10-03-Ol4 | 0.909 | 0.749 | 0.3 | 0.32 | -9.23 | -2.37 |
| 5 | ARP73-10-03-Ol5 | 0.896 | 0.718 | 0.3 | 0.32 | -9.01 | -1.68 |
| 5 | ARP73-10-03-Ol7-MI2 | 0.914 | 0.761 | 0.3 | 0.31 | -9.53 | -2.86 |
| 5 | ARP73-10-03-Ol8 | 0.895 | 0.716 | 0.3 | 0.32 | -9.29 | -1.92 |
| 5 | ARP73-10-03-Ol9-MI1 | 0.891 | 0.706 | 0.29 | 0.32 | -8.95 | -1.5 |
| 5 | ARP73-10-03-Ol9-MI2 | 0.891 | 0.706 | 0.29 | 0.32 | -8.99 | -1.53 |
| 5 | ARP73-10-03-Ol10-MI1 | 0.916 | 0.765 | 0.3 | 0.31 | -9.21 | -2.55 |
| 5 | ARP73-10-03-Ol10-MI2 | 0.916 | 0.766 | 0.3 | 0.31 | -9.5 | -2.91 |
| 5 | ARP73-10-03-Ol11 | 0.907 | 0.745 | 0.3 | 0.31 | -9.26 | -2.55 |
| 5 | ARP73-10-03-Ol12-MI1 | 0.915 | 0.763 | 0.3 | 0.31 | -9.63 | -2.99 |
| 5 | ARP73-10-03-Ol12-MI2 | 0.915 | 0.763 | 0.3 | 0.31 | -9.55 | -2.92 |
| 5 | ARP73-10-03-Ol13-MI1 | 0.9 | 0.727 | 0.3 | 0.32 | -9.2 | -2.03 |
| 5 | ARP73-10-03-Ol13-MI2 | 0.9 | 0.727 | 0.3 | 0.32 | -9.09 | -1.9 |
| 5 | ARP73-10-03-Ol14 | 0.887 | 0.697 | 0.29 | 0.32 | -9 | -1.38 |
| 5 | ARP73-10-03-Ol15 | 0.894 | 0.713 | 0.29 | 0.32 | -8.96 | -1.59 |
| 5 | ARP73-10-03-Ol16 | 0.891 | 0.706 | 0.29 | 0.32 | -9.04 | -1.59 |
| 5 | ARP73-10-03-Ol17 | 0.895 | 0.716 | 0.3 | 0.32 | -9.12 | -1.77 |
| 5 | ARP73-10-03-Ol18 | 0.901 | 0.73 | 0.3 | 0.32 | -9.08 | -1.95 |
| 5 | ARP73-10-03-Ol19-MI1 | 0.913 | 0.759 | 0.3 | 0.32 | -9.15 | -2.45 |
| 5 | ARP73-10-03-Ol19-MI2 | 0.913 | 0.759 | 0.3 | 0.31 | -9.42 | -2.77 |
| 5 | ARP73-10-03-B2(1)* | 0.892 | 0.708 | 0.29 | 0.32 | -9.07 | -1.62 |
| 5 | ARP73-10-03-128* | 0.914 | 0.76 | 0.3 | 0.31 | -9.57 | -2.95 |
| 5 | ARP73-10-03-314* | 0.9 | 0.727 | 0.3 | 0.32 | -9.25 | -2.06 |
| 5 | ARP73-10-03-324* | 0.892 | 0.708 | 0.29 | 0.32 | -8.94 | -1.46 |

| | | | | | | | |
|---|---|---|---|---|---|---|---|
| 5 | ARP73-10-03-9* | 0.894 | 0.713 | 0.29 | 0.32 | -9.04 | -1.63 |
| 5 | ARP73-10-03-15* | 0.897 | 0.719 | 0.29 | 0.32 | -8.88 | -1.6 |
| 5 | ARP73-10-03-22* | 0.904 | 0.737 | 0.3 | 0.31 | -9.27 | -2.44 |
| 5 | ARP73-10-03-23* | 0.89 | 0.703 | 0.29 | 0.32 | -8.88 | -1.37 |
| 5 | ARP73-10-03-27* | 0.904 | 0.737 | 0.3 | 0.32 | -9.24 | -2.27 |
| 5 | ARP73-10-03-39* | 0.902 | 0.729 | 0.29 | 0.32 | -8.82 | -1.44 |
| 5 | ARP73-10-03-41* | 0.908 | 0.746 | 0.3 | 0.31 | -9.12 | -2.41 |
| 5 | ARP73-10-03-114* | 0.896 | 0.718 | 0.3 | 0.32 | -9.06 | -1.72 |
| 5 | ARP73-10-03-117* | 0.901 | 0.73 | 0.3 | 0.32 | -9.27 | -2.1 |
| 5 | ARP73-10-03-296* | 0.91 | 0.751 | 0.3 | 0.31 | -9.6 | -2.78 |
| 5 | ARP73-10-03-299* | 0.9 | 0.727 | 0.3 | 0.32 | -9.32 | -2.12 |
| 5 | ARP73-10-03-115a* | 0.896 | 0.718 | 0.3 | 0.32 | -9.02 | -1.69 |
| 5 | ALV518-3-1 Ol1 | 0.861 | 0.644 | 0.29 | 0.32 | -9.03 | -1.14 |
| 5 | ALV518-3-1 Ol2 | 0.861 | 0.643 | 0.29 | 0.32 | -8.93 | -1.07 |
| 5 | ALV518-3-1 Ol3-MI1 | 0.862 | 0.647 | 0.29 | 0.32 | -9.08 | -1.23 |
| 5 | ALV518-3-1 Ol3-MI2 | 0.862 | 0.647 | 0.29 | 0.32 | -9.17 | -1.3 |
| 5 | ALV518-3-1 Ol3-MI3 | 0.862 | 0.646 | 0.29 | 0.32 | -9.06 | -1.17 |
| 5 | ALV518-3-1 Ol4-MI1 | 0.898 | 0.721 | 0.29 | 0.32 | -9.07 | -1.53 |
| 5 | ALV518-3-1 Ol4-MI2 | 0.898 | 0.722 | 0.3 | 0.32 | -9.09 | -1.69 |
| 5 | ALV518-3-1 Ol4-MI3 | 0.898 | 0.72 | 0.29 | 0.32 | -8.95 | -1.44 |
| 5 | ALV518-3-1 Ol5-MI1 | 0.872 | 0.667 | 0.29 | 0.32 | -9.3 | -1.3 |
| 5 | ALV518-3-1 Ol5-MI2 | 0.872 | 0.668 | 0.3 | 0.32 | -9.32 | -1.38 |
| 5 | ALV518-3-1 Ol6 | 0.895 | 0.715 | 0.29 | 0.32 | -9.04 | -1.66 |
| 5 | ALV518-3-1 Ol7 | 0.888 | 0.696 | 0.29 | 0.32 | -8.63 | -0.87 |
| 5 | ALV518-3-1 Ol8-MI1 | 0.9 | 0.727 | 0.3 | 0.32 | -9.04 | -1.71 |
| 5 | ALV518-3-1 Ol8-MI2 | 0.9 | 0.727 | 0.3 | 0.32 | -9.1 | -1.77 |
| 5 | ALV518-3-1 Ol9-MI1 | 0.9 | 0.72 | 0.29 | 0.32 | -8.14 | -0.91 |
| 5 | ALV518-3-1 Ol9-MI2 | 0.9 | 0.719 | 0.28 | 0.32 | -7.88 | -0.79 |
| 5 | ALV518-3-1 Ol10 | 0.866 | 0.655 | 0.29 | 0.32 | -9.17 | -1.3 |
| 5 | ALV518-3-1 Ol11 | 0.891 | 0.705 | 0.29 | 0.32 | -9.05 | -1.4 |
| 5 | ALV518-3-2-Ol1 | 0.876 | 0.67 | 0.29 | 0.32 | -9.08 | -1.11 |

| | | | | | | | |
|---|---|---|---|---|---|---|---|
| 5 | ALV518-3-2-Ol2 | 0.898 | 0.722 | 0.3 | 0.32 | -9.33 | -1.95 |
| 5 | ALV518-3-2-Ol3 | 0.858 | 0.64 | 0.29 | 0.32 | -9.39 | -1.34 |
| 5 | ALV518-3-2-Ol5 | 0.898 | 0.719 | 0.29 | 0.32 | -8.96 | -1.45 |
| 5 | ALV518-3-2-Ol6 | 0.868 | 0.664 | 0.3 | 0.32 | -9.76 | -1.79 |
| 5 | ALV518-3-3-Ol1 | 0.864 | 0.651 | 0.29 | 0.32 | -9.19 | -1.26 |
| 5 | ALV518-3-3-Ol3 | 0.873 | 0.668 | 0.29 | 0.32 | -9.3 | -1.25 |
| 5 | ALV518-3-3-Ol4 | 0.853 | 0.638 | 0.3 | 0.32 | -10.2 | -2.21 |
| 5 | ALV518-3-3-Ol5 | 0.864 | 0.653 | 0.3 | 0.32 | -9.47 | -1.47 |
| 5 | ALV518-3-3-Ol6-MI1 | 0.877 | 0.674 | 0.29 | 0.32 | -9.1 | -1.03 |
| 5 | ALV518-3-3-Ol6-MI2 | 0.877 | 0.674 | 0.29 | 0.32 | -9.05 | -1.05 |
| 5 | ALV518-3-3-Ol7-MI1 | 0.862 | 0.648 | 0.29 | 0.32 | -9.41 | -1.39 |
| 5 | ALV518-3-3-Ol7-MI2 | 0.862 | 0.648 | 0.29 | 0.32 | -9.37 | -1.39 |
| 5 | ALV518-3-3-Ol7-MI3 | 0.862 | 0.647 | 0.29 | 0.32 | -9.2 | -1.3 |
| 5 | ALV518-3-3-Ol8 | 0.862 | 0.648 | 0.29 | 0.32 | -9.29 | -1.32 |
| 5 | ALV518-3-4 Ol1 | 0.865 | 0.652 | 0.29 | 0.32 | -9.08 | -1.16 |
| 5 | ALV518-3-4 Ol2 | 0.895 | 0.715 | 0.29 | 0.32 | -9.09 | -1.77 |
| 5 | ALV518-3-4 Ol5 | 0.863 | 0.65 | 0.29 | 0.32 | -9.36 | -1.37 |
| 5 | ALV518-3-4 Ol6 | 0.873 | 0.67 | 0.3 | 0.32 | -9.48 | -1.44 |
| 5 | ALV518-3-4 Ol8-MI1 | 0.861 | 0.645 | 0.29 | 0.32 | -9.24 | -1.29 |
| 5 | ALV518-3-4 Ol8-MI2 | 0.861 | 0.648 | 0.3 | 0.33 | -9.51 | -1.44 |
| 5 | ALV518-3-4 Ol9 | 0.881 | 0.679 | 0.29 | 0.32 | -8.73 | -0.77 |
| 5 | ALV518-3-4 Ol10 | 0.892 | 0.707 | 0.29 | 0.32 | -9.06 | -1.46 |
| 5 | ALV518-3-4 Ol11-MI1 | 0.886 | 0.692 | 0.29 | 0.32 | -8.69 | -0.92 |
| 5 | ALV518-3-4 Ol11-MI2 | 0.886 | 0.692 | 0.29 | 0.32 | -8.71 | -0.92 |
| 5 | ALV518-3-4 Ol12 | 0.868 | 0.66 | 0.3 | 0.32 | -9.36 | -1.4 |
| 5 | ALV518-3-4 Ol13-MI1 | 0.866 | 0.655 | 0.29 | 0.32 | -9.19 | -1.3 |
| 5 | ALV518-3-4 Ol13-MI2 | 0.866 | 0.654 | 0.29 | 0.32 | -9.08 | -1.22 |
| 5 | ALV518-3-4 Ol14 | 0.868 | 0.661 | 0.3 | 0.32 | -9.37 | -1.41 |
| 5 | ALV518-3-4 Ol16 | 0.886 | 0.692 | 0.29 | 0.32 | -8.86 | -1.06 |
| 5 | ALV518-3-4 Ol17 | 0.883 | 0.683 | 0.29 | 0.32 | -8.58 | -0.7 |
| 5 | ALV518-3-4 Ol18 | 0.873 | 0.667 | 0.29 | 0.32 | -9.07 | -1.16 |

| | | | | | | | |
|---|---|---|---|---|---|---|---|
| 5 | ALV519-2-3-Ol1 | 0.896 | 0.707 | 0.28 | 0.31 | -8.44 | -0.8 |
| 5 | ALV519-2-3-Ol3-MI1 | 0.903 | 0.72 | 0.28 | 0.31 | -8.3 | -0.7 |
| 5 | ALV519-2-3-Ol3-MI2 | 0.903 | 0.72 | 0.28 | 0.31 | -8.34 | -0.61 |
| 5 | ALV519-2-3-Ol5 | 0.901 | 0.719 | 0.28 | 0.31 | -8.86 | -1.07 |
| 5 | ALV519-2-3-Ol6 | 0.883 | 0.689 | 0.29 | 0.32 | -8.94 | -1.14 |
| 5 | ALV519-2-3-Ol7-MI1 | 0.895 | 0.71 | 0.29 | 0.32 | -8.63 | -0.89 |
| 5 | ALV519-2-3-Ol7-MI2 | 0.895 | 0.706 | 0.28 | 0.31 | -8.57 | -0.9 |
| 5 | ALV519-2-3-Ol8 | 0.9 | 0.716 | 0.28 | 0.32 | -8.31 | -0.73 |
| 5 | ALV519-2-3-Ol9 | 0.895 | 0.706 | 0.28 | 0.31 | -8.54 | -0.9 |
| 5 | ALV519-2-3-Ol10 | 0.887 | 0.689 | 0.28 | 0.32 | -8.6 | -0.77 |
| 5 | ALV519-4-1-Ol1 | 0.895 | 0.712 | 0.29 | 0.32 | -8.59 | -0.96 |
| 5 | ALV519-4-1-Ol2 | 0.914 | 0.76 | 0.3 | 0.31 | -10.1 | -3.53 |
| 5 | ALV519-4-1-Ol3 | 0.913 | 0.759 | 0.3 | 0.31 | -10.8 | -4.3 |
| 5 | ALV519-4-1-Ol4 | 0.896 | 0.713 | 0.29 | 0.32 | -8.41 | -0.86 |
| 5 | ALV519-4-1-Ol5 | 0.896 | 0.713 | 0.29 | 0.32 | -8.99 | -0.99 |
| 5 | ALV519-4-1-Ol6-MI1 | 0.886 | 0.686 | 0.28 | 0.32 | -8.48 | -0.77 |
| 5 | ALV519-4-1-Ol6-MI2 | 0.886 | 0.686 | 0.28 | 0.32 | -8.45 | -0.71 |
| 5 | ALV519-4-1-Ol7 | 0.898 | 0.71 | 0.28 | 0.31 | -8.15 | -0.65 |
| 5 | ALV519-4-1-Ol8-MI1 | 0.893 | 0.7 | 0.28 | 0.32 | -8.19 | -0.55 |
| 5 | ALV519-4-1-Ol8-MI2 | 0.893 | 0.701 | 0.28 | 0.32 | -8.21 | -0.57 |
| 5 | ALV519-4-1-Ol9 | 0.895 | 0.701 | 0.28 | 0.31 | -8.24 | -0.62 |
| 5 | ALV519-4-1-Ol10 | 0.884 | 0.687 | 0.29 | 0.32 | -8.74 | -1.13 |
| 5 | ALV519-4-1-Ol11 | 0.888 | 0.692 | 0.28 | 0.32 | -8.36 | -0.67 |
| 5 | ALV521-1 Ol1 | 0.882 | 0.684 | 0.29 | 0.32 | -9.01 | -1.05 |
| 5 | ALV521-1 Ol2-MI1 | 0.881 | 0.682 | 0.29 | 0.32 | -8.93 | -0.99 |
| 5 | ALV521-1 Ol2-MI2 | 0.881 | 0.683 | 0.29 | 0.32 | -9.08 | -1.08 |
| 5 | ALV521-1 Ol3-MI1 | 0.869 | 0.659 | 0.29 | 0.33 | -9.48 | -1.14 |
| 5 | ALV521-1 Ol3-MI2 | 0.869 | 0.66 | 0.29 | 0.33 | -9.65 | -1.14 |
| 5 | ALV521-1 Ol4 | 0.872 | 0.663 | 0.29 | 0.32 | -9.19 | -1.08 |
| 5 | ALV521-1 Ol6 | 0.874 | 0.666 | 0.29 | 0.32 | -8.95 | -0.93 |
| 5 | ALV521-1 Ol7 | 0.879 | 0.68 | 0.29 | 0.32 | -9.21 | -1.17 |

| | | | | | | | |
|---|---|---|---|---|---|---|---|
| 5 | ALV521-1 Ol8-MI1 | 0.873 | 0.665 | 0.29 | 0.32 | -9.16 | -0.99 |
| 5 | ALV521-1 Ol9-MI1 | 0.881 | 0.681 | 0.29 | 0.32 | -8.87 | -0.97 |
| 5 | ALV521-1 Ol9-MI2 | 0.881 | 0.679 | 0.29 | 0.32 | -8.81 | -0.85 |
| 5 | ALV521-1 Ol9-MI3 | 0.881 | 0.681 | 0.29 | 0.32 | -8.98 | -1.03 |
| 5 | ALV521-1 Ol9-MI4 | 0.884 | 0.686 | 0.29 | 0.32 | -8.9 | -1.01 |
| 5 | ALV521-1 Ol10 | 0.884 | 0.688 | 0.29 | 0.32 | -8.87 | -1.03 |
| 5 | ALV521-1 Ol11 | 0.882 | 0.681 | 0.29 | 0.32 | -8.15 | -0.82 |
| 5 | ALV521-1 Ol13 | 0.882 | 0.685 | 0.29 | 0.32 | -9.04 | -1.25 |
| 5 | ALV521-1 Ol14 | 0.884 | 0.688 | 0.29 | 0.32 | -8.82 | -1.07 |
| 5 | ALV521-1 Ol15 | 0.881 | 0.68 | 0.29 | 0.32 | -8.93 | -0.9 |
| 5 | ALV521-1 Ol16 | 0.88 | 0.682 | 0.29 | 0.32 | -8.97 | -1.18 |
| 5 | ALV524-4 Ol2 | 0.882 | 0.683 | 0.29 | 0.32 | -8.94 | -1.03 |
| 5 | ALV524-4 Ol3 | 0.883 | 0.686 | 0.29 | 0.32 | -8.56 | -1.1 |
| 5 | ALV524-4 Ol4 | 0.882 | 0.682 | 0.29 | 0.32 | -8.79 | -1.12 |
| 5 | ALV524-4 Ol5-MI1 | 0.882 | 0.682 | 0.29 | 0.32 | -8.89 | -0.99 |
| 5 | ALV524-4 Ol5-MI2 | 0.882 | 0.683 | 0.29 | 0.32 | -8.94 | -1.01 |
| 5 | ALV524-4 Ol7-MI1 | 0.882 | 0.681 | 0.29 | 0.32 | -8.89 | -0.97 |
| 5 | ALV524-4 Ol7-MI2 | 0.882 | 0.683 | 0.29 | 0.32 | -9.15 | -0.93 |
| 5 | ALV524-4 Ol7-MI3 | 0.882 | 0.685 | 0.29 | 0.32 | -9.22 | -1.13 |
| 5 | ALV524-4 Ol8 | 0.863 | 0.645 | 0.29 | 0.32 | -9.59 | -1.08 |
| 5 | ALV524-4 Ol9 | 0.884 | 0.689 | 0.29 | 0.32 | -9.17 | -1.09 |
| 5 | ALV524-4 Ol10 | 0.885 | 0.686 | 0.28 | 0.32 | -8.91 | -1.03 |
| 5 | ALV524-4 Ol11 | 0.884 | 0.687 | 0.29 | 0.32 | -8.91 | -0.99 |
| 5 | ALV524-4 Ol12 | 0.882 | 0.682 | 0.29 | 0.32 | -8.79 | -0.96 |
| 5 | ALV524-4 Ol13 | 0.883 | 0.685 | 0.29 | 0.32 | -9.01 | -1.15 |
| 5 | ALV524-4 Ol14 | 0.883 | 0.683 | 0.29 | 0.32 | -8.74 | -0.89 |
| 5 | ALV527-1-Ol1-MI1 | 0.883 | 0.677 | 0.28 | 0.31 | -8.49 | -0.84 |
| 5 | ALV527-1-Ol1-MI2 | 0.883 | 0.677 | 0.28 | 0.31 | -8.46 | -0.82 |
| 5 | ALV527-1-Ol2-MI1 | 0.898 | 0.716 | 0.29 | 0.32 | -8.49 | -0.87 |
| 5 | ALV527-1-Ol2-MI2 | 0.898 | 0.716 | 0.29 | 0.32 | -8.42 | -0.81 |
| 5 | ALV527-1-Ol3 | 0.887 | 0.687 | 0.28 | 0.31 | -8.58 | -0.91 |

| | | | | | | | |
|---|---|---|---|---|---|---|---|
| 5 | ALV527-1-Ol4 | 0.892 | 0.697 | 0.28 | 0.31 | -8.1 | -0.57 |
| 5 | ALV527-1-Ol5 | 0.897 | 0.714 | 0.29 | 0.32 | -8.32 | -0.87 |
| 5 | ALV527-1-Ol6-MI1 | 0.897 | 0.713 | 0.29 | 0.32 | -8.34 | -0.8 |
| 5 | ALV527-1-Ol6-MI2 | 0.897 | 0.712 | 0.28 | 0.32 | -8.19 | -0.65 |
| 5 | ALV527-1-Ol7 | 0.885 | 0.691 | 0.29 | 0.32 | -8.67 | -0.93 |
| 5 | ARP74-11-18-Ol1 | 0.893 | 0.707 | 0.29 | 0.32 | -8.82 | -1.2 |
| 5 | ARP74-11-18-Ol2 | 0.898 | 0.721 | 0.29 | 0.32 | -8.84 | -1.47 |
| 5 | ARP74-11-18-Ol3 | 0.9 | 0.726 | 0.29 | 0.32 | -9.09 | -1.7 |
| 5 | ARP74-11-18-Ol4 | 0.896 | 0.716 | 0.29 | 0.32 | -9.14 | -1.6 |
| 5 | ARP74-11-18-Ol5-MI1 | 0.904 | 0.736 | 0.3 | 0.32 | -9.24 | -2.04 |
| 5 | ARP74-11-18-Ol6-MI1 | 0.903 | 0.734 | 0.3 | 0.32 | -9.45 | -2.31 |
| 5 | ARP74-11-18-Ol6-MI2 | 0.903 | 0.734 | 0.3 | 0.31 | -9.55 | -2.42 |
| 5 | ARP74-11-18-Ol7-MI1 | 0.903 | 0.734 | 0.3 | 0.32 | -9.26 | -2.11 |
| 5 | ARP74-11-18-Ol7-MI2 | 0.903 | 0.734 | 0.3 | 0.32 | -9.34 | -2.18 |
| 5 | ARP74-11-18-Ol8 | 0.886 | 0.692 | 0.29 | 0.33 | -8.53 | -0.8 |
| 5 | ARP74-11-18-Ol9 | 0.899 | 0.724 | 0.29 | 0.32 | -8.97 | -1.68 |
| 5 | ARP74-11-18-Ol10 | 0.897 | 0.719 | 0.29 | 0.32 | -9.15 | -1.77 |
| 5 | ARP74-11-18-Ol11 | 0.901 | 0.728 | 0.29 | 0.32 | -9.16 | -1.63 |
| 5 | CH31-DR8-Ol1 | 0.894 | 0.705 | 0.28 | 0.32 | -8.22 | -0.64 |
| 5 | CH31-DR8-Ol2 | 0.905 | 0.74 | 0.3 | 0.32 | -9.43 | -2.32 |
| 5 | CH31-DR8-Ol3-MI1 | 0.892 | 0.707 | 0.29 | 0.32 | -8.81 | -1.28 |
| 5 | CH31-DR8-Ol3-MI2 | 0.892 | 0.707 | 0.29 | 0.32 | -8.87 | -1.33 |
| 5 | CH31-DR8-Ol4 | 0.913 | 0.759 | 0.3 | 0.31 | -9.89 | -3.09 |
| 5 | CH31-DR8-Ol5 | 0.891 | 0.706 | 0.29 | 0.32 | -8.93 | -1.38 |
| 5 | CH31-DR8-Ol6-MI1 | 0.91 | 0.752 | 0.3 | 0.31 | -9.79 | -3.05 |
| 5 | CH31-DR8-Ol6-MI2 | 0.91 | 0.751 | 0.3 | 0.32 | -9.22 | -2.31 |
| 5 | CH31-DR8-Ol7-MI1 | 0.904 | 0.737 | 0.3 | 0.32 | -9.34 | -2.23 |
| 5 | CH31-DR8-Ol7-MI2 | 0.904 | 0.737 | 0.3 | 0.32 | -9.06 | -1.92 |
| 5 | CH31-DR8-Ol7-MI3 | 0.904 | 0.737 | 0.3 | 0.32 | -9.23 | -2.13 |
| 5 | CH31-DR8-Ol7-MI4 | 0.904 | 0.737 | 0.3 | 0.32 | -9.24 | -2.12 |
| 5 | CH31-DR8-Ol8 | 0.91 | 0.752 | 0.3 | 0.31 | -9.48 | -2.75 |

| | | | | | | | |
|---|---|---|---|---|---|---|---|
| 5 | CH31-DR8-Ol9-MI1 | 0.903 | 0.734 | 0.3 | 0.32 | -9.2 | -2.02 |
| 5 | CH31-DR8-Ol9-MI2 | 0.903 | 0.734 | 0.3 | 0.32 | -9.29 | -2.14 |
| 5 | CH31-DR8-Ol10 | 0.899 | 0.726 | 0.3 | 0.32 | -9.2 | -1.9 |
| 5 | CH31-DR8-Ol11-MI1 | 0.899 | 0.725 | 0.3 | 0.32 | -9.22 | -1.93 |
| 5 | CH31-DR8-Ol11-MI2 | 0.899 | 0.725 | 0.3 | 0.32 | -9.22 | -1.91 |
| 5 | CH31-DR8-Ol11-MI3 | 0.899 | 0.725 | 0.3 | 0.32 | -9.13 | -1.81 |
| 5 | G103-20-6-Ol4 | 0.899 | 0.723 | 0.29 | 0.32 | -9.02 | -1.61 |
| 5 | G103-20-6-Ol7 | 0.883 | 0.684 | 0.29 | 0.32 | -8.77 | -0.81 |
| 5 | G103-20-6-Ol8 | 0.888 | 0.696 | 0.29 | 0.32 | -8.96 | -1.17 |
| 5 | G103-20-6-Ol9 | 0.897 | 0.72 | 0.29 | 0.32 | -9.19 | -1.71 |
| 5 | G103-20-6-Ol10 | 0.898 | 0.721 | 0.29 | 0.32 | -9.17 | -1.7 |
| 5 | G103-20-6-Ol12 | 0.898 | 0.721 | 0.29 | 0.32 | -9.15 | -1.71 |
| 5 | G103-20-6-Ol14 | 0.898 | 0.72 | 0.29 | 0.32 | -8.61 | -1.26 |
| 5 | NR-DR3-3-Ol1 | 0.899 | 0.724 | 0.29 | 0.32 | -9.04 | -1.63 |
| 5 | NR-DR3-3-Ol2 | 0.903 | 0.735 | 0.3 | 0.32 | -9.32 | -2.07 |
| 5 | NR-DR3-3-Ol3 | 0.9 | 0.726 | 0.29 | 0.32 | -9.08 | -1.58 |
| 5 | NR-DR3-3-Ol5 | 0.904 | 0.736 | 0.3 | 0.32 | -10.1 | -1.88 |
| 5 | NR-DR3-3-Ol6 | 0.903 | 0.734 | 0.3 | 0.32 | -9.22 | -1.83 |
| 5 | NR-DR3-3-Ol7 | 0.907 | 0.744 | 0.3 | 0.32 | -9.43 | -2.28 |
| 5 | NR-DR3-3-Ol8 | 0.907 | 0.743 | 0.3 | 0.32 | -9.06 | -1.96 |
| 5 | NR-DR3-3-Ol9 | 0.903 | 0.734 | 0.3 | 0.32 | -8.95 | -1.79 |
| 5 | m1-1 | 0.893 | 0.71 | 0.29 | 0.32 | -8.69 | -1.11 |
| 5 | m1-2 | 0.893 | 0.7 | 0.28 | 0.31 | -8.42 | -0.88 |
| 5 | m1-3 | 0.894 | 0.703 | 0.28 | 0.32 | -8.46 | -0.86 |
| 5 | m1-4 | 0.888 | 0.693 | 0.28 | 0.32 | -8.67 | -0.98 |
| 5 | m1-5 | 0.881 | 0.685 | 0.29 | 0.33 | -8.9 | -1.05 |
| 5 | m2-1 | 0.893 | 0.704 | 0.28 | 0.32 | -8.78 | -0.85 |
| 5 | m2-2 | 0.896 | 0.713 | 0.29 | 0.32 | -8.88 | -1.2 |
| 5 | m2-4 | 0.881 | 0.686 | 0.29 | 0.32 | -8.97 | -1.17 |
| 5 | m2-5 | 0.906 | 0.742 | 0.3 | 0.32 | -9.41 | -2.33 |
| 5 | m2-6 | 0.886 | 0.694 | 0.29 | 0.32 | -8.9 | -1.06 |

| | | | | | | | |
|---|---|---|---|---|---|---|---|
| 5 | m2-7 | 0.905 | 0.738 | 0.3 | 0.32 | -9.05 | -1.82 |
| 5 | m2-8 | 0.894 | 0.704 | 0.28 | 0.31 | -8.27 | -0.94 |
| 5 | m2-9 | 0.889 | 0.701 | 0.29 | 0.32 | -8.83 | -1.14 |
| 5 | m2-10 | 0.912 | 0.756 | 0.3 | 0.32 | -9.17 | -2.2 |
| 5 | m2-11 | 0.887 | 0.692 | 0.29 | 0.32 | -8.6 | -1.09 |
| 5 | m3-1 | 0.894 | 0.702 | 0.28 | 0.31 | -7.89 | -0.7 |
| 5 | m3-2 | 0.898 | 0.714 | 0.28 | 0.32 | -8.53 | -0.79 |
| 5 | m3-3 | 0.884 | 0.687 | 0.29 | 0.32 | -8.38 | -0.81 |
| 5 | m3-4 | 0.898 | 0.712 | 0.28 | 0.31 | -7.89 | -0.69 |
| 5 | m3-5 | 0.897 | 0.711 | 0.28 | 0.32 | -8.32 | -0.72 |
| 5 | m3-6 | 0.896 | 0.71 | 0.28 | 0.32 | -8.25 | -0.93 |
| 5 | m3-7 | 0.896 | 0.707 | 0.28 | 0.32 | -8.37 | -0.67 |
| 5 | 2 | 0.893 | 0.71 | 0.29 | 0.32 | -9.03 | -1.58 |
| 5 | 4 | 0.893 | 0.71 | 0.29 | 0.32 | -8.92 | -1.48 |
| 5 | 5 | 0.893 | 0.71 | 0.29 | 0.32 | -8.89 | -1.49 |
| 5 | 6 | 0.893 | 0.709 | 0.29 | 0.32 | -8.97 | -1.54 |
| 5 | 11 | 0.913 | 0.758 | 0.3 | 0.31 | -9.35 | -2.64 |
| 5 | 17 | 0.892 | 0.708 | 0.29 | 0.32 | -9.02 | -1.55 |
| 5 | 18 | 0.898 | 0.724 | 0.3 | 0.32 | -9.3 | -2.04 |
| 5 | 19 | 0.898 | 0.724 | 0.3 | 0.32 | -9.3 | -2.08 |
| 5 | 114 | 0.896 | 0.718 | 0.3 | 0.32 | -9.1 | -1.77 |
| 5 | 115a | 0.896 | 0.718 | 0.3 | 0.32 | -9.06 | -1.73 |
| 5 | 115b | 0.896 | 0.718 | 0.3 | 0.32 | -9.12 | -1.8 |
| 5 | 117 | 0.901 | 0.73 | 0.3 | 0.32 | -9.34 | -2.17 |
| 5 | 128 | 0.903 | 0.734 | 0.3 | 0.31 | -9.46 | -2.41 |
| 5 | 271 | 0.899 | 0.725 | 0.3 | 0.32 | -9.2 | -1.98 |
| 5 | 273 | 0.904 | 0.738 | 0.3 | 0.32 | -9.47 | -2.37 |
| 5 | 277 | 0.891 | 0.706 | 0.29 | 0.32 | -9.23 | -1.77 |
| 5 | 282 | 0.893 | 0.711 | 0.3 | 0.32 | -9.4 | -1.95 |
| 5 | 283 | 0.893 | 0.711 | 0.3 | 0.32 | -9.28 | -1.84 |
| 5 | 285 | 0.907 | 0.744 | 0.3 | 0.32 | -9.29 | -2.23 |

| | | | | | | | |
|---|---|---|---|---|---|---|---|
| 5 | 286 | 0.907 | 0.744 | 0.3 | 0.31 | -9.64 | -2.71 |
| 5 | 289 | 0.915 | 0.764 | 0.3 | 0.31 | -9.83 | -3.27 |
| 5 | 290 | 0.91 | 0.753 | 0.3 | 0.31 | -10.1 | -3.26 |
| 5 | 292 | 0.901 | 0.729 | 0.29 | 0.32 | -9.06 | -1.76 |
| 5 | 294 | 0.891 | 0.704 | 0.29 | 0.32 | -8.87 | -1.38 |
| 5 | 296 | 0.91 | 0.751 | 0.3 | 0.31 | -9.71 | -2.9 |
| 5 | 297 | 0.91 | 0.751 | 0.3 | 0.31 | -9.65 | -2.83 |
| 5 | 299 | 0.9 | 0.728 | 0.3 | 0.32 | -9.66 | -2.49 |
| 5 | 301 | 0.912 | 0.755 | 0.3 | 0.31 | -9.57 | -2.89 |
| 5 | 302 | 0.922 | 0.78 | 0.3 | 0.31 | -10.2 | -3.83 |
| 5 | 306 | 0.894 | 0.713 | 0.29 | 0.32 | -9.04 | -1.64 |
| 5 | 311 | 0.9 | 0.727 | 0.3 | 0.32 | -9.04 | -1.84 |
| 5 | 314 | 0.904 | 0.737 | 0.3 | 0.31 | -9.53 | -2.49 |
| 5 | 319 | 0.914 | 0.762 | 0.3 | 0.31 | -9.99 | -3.35 |
| 5 | 324 | 0.904 | 0.737 | 0.3 | 0.32 | -9.29 | -2.23 |
| 5 | 337 | 0.916 | 0.764 | 0.3 | 0.31 | -9.46 | -2.89 |
| 5 | 357 | 0.885 | 0.693 | 0.29 | 0.32 | -9.21 | -1.56 |
| 5 | 1 | 0.895 | 0.716 | 0.3 | 0.32 | -9.26 | -1.88 |
| 5 | 2 | 0.898 | 0.724 | 0.3 | 0.32 | -9.37 | -2.14 |
| 5 | 3 | 0.894 | 0.713 | 0.29 | 0.32 | -9.07 | -1.67 |
| 5 | 4a | 0.908 | 0.746 | 0.3 | 0.31 | -9.44 | -2.55 |
| 5 | 4b | 0.908 | 0.746 | 0.3 | 0.32 | -9.36 | -2.46 |
| 5 | 5 | 0.908 | 0.746 | 0.3 | 0.32 | -9.29 | -2.39 |
| 5 | 6 | 0.912 | 0.756 | 0.3 | 0.31 | -9.45 | -2.72 |
| 5 | 7 | 0.914 | 0.76 | 0.3 | 0.31 | -9.31 | -2.62 |
| 5 | 8 | 0.893 | 0.711 | 0.3 | 0.32 | -9 | -1.57 |
| 5 | 9 | 0.894 | 0.711 | 0.29 | 0.32 | -8.86 | -1.44 |
| 5 | 10 | 0.907 | 0.742 | 0.3 | 0.32 | -8.87 | -1.93 |
| 5 | 11 | 0.907 | 0.743 | 0.3 | 0.32 | -8.98 | -2.06 |
| 5 | 12 | 0.912 | 0.755 | 0.3 | 0.31 | -9.16 | -2.41 |
| 5 | 13 | 0.913 | 0.758 | 0.3 | 0.31 | -9.26 | -2.55 |

| | | | | | | | |
|---|---|---|---|---|---|---|---|
| 5 | 14 | 0.893 | 0.711 | 0.3 | 0.32 | -9.12 | -1.69 |
| 5 | 15 | 0.897 | 0.719 | 0.29 | 0.32 | -9.03 | -1.65 |
| 5 | 16 | 0.899 | 0.725 | 0.3 | 0.32 | -9.2 | -1.97 |
| 5 | 17 | 0.911 | 0.753 | 0.3 | 0.31 | -9.28 | -2.51 |
| 5 | 18 | 0.898 | 0.721 | 0.29 | 0.32 | -8.95 | -1.69 |
| 5 | 19 | 0.893 | 0.711 | 0.3 | 0.32 | -9.08 | -1.67 |
| 5 | 20 g | 0.913 | 0.758 | 0.3 | 0.31 | -9.62 | -2.92 |
| 5 | 20 p | 0.913 | 0.757 | 0.3 | 0.31 | -9.41 | -2.71 |
| 5 | 21 | 0.904 | 0.736 | 0.3 | 0.32 | -8.93 | -1.91 |
| 5 | 22 | 0.904 | 0.736 | 0.3 | 0.32 | -9.05 | -2.02 |
| 5 | 23 | 0.89 | 0.703 | 0.29 | 0.32 | -8.93 | -1.42 |
| 5 | 24 | 0.894 | 0.715 | 0.3 | 0.32 | -9.24 | -1.86 |
| 5 | 25 | 0.89 | 0.703 | 0.29 | 0.32 | -8.86 | -1.32 |
| 5 | 26 | 0.905 | 0.738 | 0.3 | 0.31 | -9.29 | -2.31 |
| 5 | 27 | 0.904 | 0.737 | 0.3 | 0.32 | -9.37 | -2.33 |
| 5 | 28 | 0.904 | 0.737 | 0.3 | 0.32 | -9.31 | -2.27 |
| 5 | 29 | 0.904 | 0.737 | 0.3 | 0.31 | -9.69 | -2.69 |
| 5 | 30 | 0.89 | 0.703 | 0.29 | 0.32 | -8.94 | -1.4 |
| 5 | 31 | 0.89 | 0.703 | 0.29 | 0.32 | -9.01 | -1.48 |
| 5 | 32 | 0.89 | 0.703 | 0.29 | 0.32 | -9.01 | -1.47 |
| 5 | 33 | 0.9 | 0.727 | 0.3 | 0.32 | -9.08 | -1.88 |
| 5 | 34 | 0.887 | 0.695 | 0.29 | 0.32 | -8.75 | -1.13 |
| 5 | 35 | 0.887 | 0.695 | 0.29 | 0.32 | -8.86 | -1.22 |
| 5 | 36 | 0.887 | 0.695 | 0.29 | 0.32 | -8.88 | -1.24 |
| 5 | 37 | 0.883 | 0.686 | 0.29 | 0.32 | -8.84 | -1.08 |
| 5 | 38 | 0.905 | 0.738 | 0.3 | 0.32 | -9.09 | -2.1 |
| 5 | 39 | 0.902 | 0.733 | 0.3 | 0.32 | -9.37 | -2.26 |
| 5 | 40 | 0.894 | 0.714 | 0.3 | 0.32 | -9.2 | -1.8 |
| 5 | 41 | 0.908 | 0.746 | 0.3 | 0.32 | -9.26 | -2.37 |
| 5 | a | 0.9 | 0.727 | 0.3 | 0.32 | -9.16 | -1.96 |
| 5 | b | 0.9 | 0.727 | 0.3 | 0.32 | -9.08 | -1.95 |

| | | | | | | | |
|---|---|---|---|---|---|---|---|
| 5 | c | 0.9 | 0.727 | 0.3 | 0.32 | -9.07 | -1.89 |
| 5 | d | 0.9 | 0.727 | 0.3 | 0.32 | -9.15 | -1.95 |
| 5 | e | 0.9 | 0.727 | 0.3 | 0.32 | -9.2 | -2 |
| 5 | f | 0.9 | 0.727 | 0.3 | 0.32 | -9.11 | -1.95 |
| 5 | B2(1) | 0.892 | 0.708 | 0.29 | 0.32 | -9.12 | -1.67 |
| 5 | B2(2) | 0.892 | 0.708 | 0.29 | 0.32 | -9.07 | -1.64 |
| 5 | D3(1) | 0.904 | 0.737 | 0.3 | 0.32 | -9.19 | -2.17 |
| 5 | D3(2) | 0.904 | 0.737 | 0.3 | 0.32 | -9.25 | -2.24 |
| 5 | D3(3) | 0.904 | 0.737 | 0.3 | 0.32 | -9.28 | -2.26 |
| 5 | D3(4) | 0.904 | 0.737 | 0.3 | 0.32 | -9.22 | -2.2 |